CHAPTER FOUR

^{1}H NMR Spectroscopy and MR Imaging with Hyperpolarised Substances

Dirk Graafen[*,†], Sandro Ebert[*], Oliver Neudert[*], Lisandro Buljubasich[‡], María Belén Franzoni[‡], Jan Falk Dechent[*], Kerstin Münnemann[*]

[*]Max Planck Institute for Polymer Research, Mainz, Germany
[†]Department of Radiology, Johannes Gutenberg University Medical Center, Mainz, Germany
[‡]FAMAF Universidad Nacional de Córdoba, IFEG CONICET, X5016LAE Córdoba, Argentina

Contents

Abstract

Despite their wide applicability in natural sciences, NMR and MRI still suffer from their inherently low sensitivity. This can be overcome by hyperpolarisation techniques, such as parahydrogen-induced polarisation and dynamic nuclear polarisation. Here, we focus on the generation of ^{1}H-hyperpolarised substances with both methods. We especially address the severe lifetime issue of the accomplished ^{1}H hyperpolarisation by demonstrating the production of hyperpolarised liquids in a continuous flow fashion and the storage of hyperpolarisation in slowly relaxing singlet states. Another problem of

Annual Reports on NMR Spectroscopy, Volume 82
ISSN 0066-4103
http://dx.doi.org/10.1016/B978-0-12-800184-4.00004-7

hyperpolarised proton NMR and MRI is the generation of contrast between a small amount of hyperpolarised molecules and a vast thermal background signal. In this contribution, we show the possibility to use the special signal pattern that is inherent to the hyperpolarisation method to generate excellent MRI contrast which may open up unprecedented opportunities to use the standard MRI nucleus ^{1}H, for example, biomedical applications in future.

Keywords: PHIP, DNP, NMR, MRI, Hyperpolarisation, Polarising agents, Signal enhancement, Singlet states, Continuous hyperpolarisation

1. INTRODUCTION

Despite the widespread applications of NMR and MRI that have evolved in chemistry, biology, physics and medicine and even though major improvements were achieved by the use of very high magnetic fields and optimised hardware, some applications are still impractical due to the comparatively low sensitivity of the method. However, there are several techniques that allow to overcome the inherently low nuclear spin polarisation and to provide large signal enhancements through the creation of a non-equilibrium hyperpolarised state. Among them, there are dynamic nuclear polarisation (DNP) [1,2], parahydrogen-induced polarisation (PHIP) [3–5] and the laser-driven polarisation of noble gases [6–8]. By exploiting signal enhancements of up to 5 orders of magnitude, these methods enable new possibilities for the real-time investigation of fast, dynamic processes and allow for the sensitive detection of significantly reduced sample amounts, dilute molecular tracers or low-abundance nuclear spins.

Especially magnetic resonance imaging (MRI) techniques have benefitted from the hyperpolarisation of ^{13}C achievable by DNP [9]. This technique has enabled MRI detection of dilute nuclear species, allowing for the detection of malignant tissue [10], the investigation of metabolic pathways [11,12] or *in vivo* pH mapping [13]. Other applications of hyperpolarised nuclear spins involve the investigation of fast chemical reactions using ^{13}C-DNP [14], PHIP [15] or hyperpolarised ^{129}Xe [16]. Further applications are envisaged for catalysis and reaction monitoring, the investigation of biological macromolecules and enzymatic reactions as well as perfusion MRI and metabolic MRI.

Most of the present applications of hyperpolarisation for MRI are based on ^{13}C nuclear spins. This approach provides a comparatively long lifetime of the hyperpolarised state, a large chemical shift range and, most notably,

negligible background signal. However, the requirement for additional, non-standard hardware to enable ^{13}C detection on clinical MRI scanners poses a major hindrance for more widespread applications. Furthermore, due to the very low natural abundance, expensive ^{13}C-enriched substances are usually needed despite large signal enhancements. Applications involving hyperpolarised ^{1}H nuclear spins, on the other hand, are feasible with standard equipment, benefit from even larger sensitivity due to the larger gyromagnetic ratio and exhibit almost 100% natural abundance. The latter fact, of course, results in a much lower contrast for MRI and may hinder the detection of small amounts of molecules against a large background signal. However, specific properties of the hyperpolarised state can be exploited to distinguish between thermally polarised and hyperpolarised signal. Overhauser DNP, for example, is usually characterised by an inversion of the initial polarisation, that is, the hyperpolarised signal exhibits a 180° phase shift, allowing for the distinction of hyperpolarised and thermally polarised signal [17]. PHIP, on the other hand, creates antiphase signals, which normally would lead to major signal cancellation and practically zero image intensity for standard MRI experiments. However, the evolution of the signal phase under J-coupling can be used to rephase the PHIP signal, generating a remarkable contrast even in the presence of a large background signal [18].

Another major hindrance for the application of ^{1}H hyperpolarisation in MRI is the presence of very effective spin-lattice relaxation mechanisms in liquids, limiting the lifetime of the hyperpolarised state to several seconds. This limit, however, can be overcome by exploiting the much longer lifetime of nuclear singlet states [19–21], which is typically on the order of several minutes. For DNP, the hyperpolarisation can be stored in a slowly relaxing singlet state by the application of an rf pulse sequence known as M2S [22,23] developed by Levitt and coworkers. PHIP, on the other hand, is based on the singlet spin order of parahydrogen (pH_2) and therefore could naturally create a nuclear spin-singlet state on the target molecule. It was shown that this state can be preserved both at low [24,25] and high magnetic fields [26], resulting in up to 1 order of magnitude higher relaxation times. At low fields, the method is based on the creation of a strongly coupled state in which the singlet state is an eigenstate of the spin system and therefore naturally preserved. The method for high fields makes use of symmetrical molecules in which the pH_2 atoms are chemically equivalent and therefore strongly coupled in every magnetic field. Furthermore, it was shown that the necessary conversion from the NMR-silent singlet state to a detectable triplet state can be achieved using a field-cycling method [27], based on

singlet–triplet level anti-crossings at a particular magnetic field, or by scaling the chemical shift Hamiltonian [28], using long off-resonant rf pulses.

A different approach to compensate for the lifetime limitation is based on the continuous production of hyperpolarised substance. For Overhauser DNP, this can be achieved using immobilised radicals in combination with a liquid flow setup, whereas continuous hyperpolarisation by PHIP can be realised by providing a continuous supply of parahydrogen through hollow fibre membranes [17]. While this approach might not be suitable for *in vivo* MRI applications or the investigation of slow metabolic processes; however, it can provide a way to realise hyperpolarised 2D-NMR spectroscopy.

DNP is a method that creates a non-equilibrium population of nuclear spin energy levels by making use of the much higher thermal equilibrium polarisation of electron spins [29]. This can be achieved by adding a radical to the sample in concentrations of typically 1–40 mmol/l. Electron spin polarisation is transferred by irradiating the sample with microwave (MW) radiation near the electron spin Larmor frequency. The effect was first predicted 1953 by Overhauser [1] and extensively studied in the following decades. The findings of these earlier works are summarised in several review articles [2,29–32]. In the last decade, DNP has experienced a revival inspired by technical improvements of the MW hardware and new methods like dissolution DNP [9]. Today, several DNP techniques exist that can produce hyperpolarised molecules: *In situ* methods, where the same magnet is used for DNP polarisation and NMR detection, are applied for liquid-state DNP [33,34] both at moderate [35,36] and high magnetic fields [37–39] as well as for solid-state DNP [40,41]. *Ex situ* methods employ different magnets for polarisation and detection and use either a flow setup [17,42,43] or a shuttle mechanism [44] for sample transfer. Here, the samples are polarised in a moderate magnetic field of typically 0.35 T, which is optimised for effective polarisation transfer, and transported to a higher magnetic field for NMR detection with optimal sensitivity and spectral resolution. Another *ex situ* approach is dissolution DNP [9], where frozen samples are polarised at high magnetic fields and temperatures of around 1 K and are afterwards quickly dissolved in a hot solvent to produce a hyperpolarised liquid sample at room temperature. While dissolution or freezing methods, which are based on solid-state DNP effects [45], can provide very large signal enhancements of around 4 orders of magnitude, they cannot be used for repeated experiments due to the experimental time required by the polarisation process, which can last up to a few hours. In contrast, methods using the Overhauser effect [1,29], that is, polarisation in the liquid-state, reach maximum

enhancement within several seconds and therefore are well suited for continuous production of hyperpolarised liquids in a flow setup.

An early application of *in situ* Overhauser DNP for MRI is proton electron double resonance imaging (PEDRI) [46–48], which was first demonstrated in 1988 by Lurie *et al.* [48]. In order to avoid dielectric losses and strong sample heating, MW frequencies are limited to about 560 MHz for biological samples, corresponding to a magnetic field of 20 mT. Therefore, PEDRI is usually combined with magnetic field cycling, where polarisation is typically performed at around 10 mT and NMR detection is done at up to 587 mT [49].

PHIP was discovered roughly 30 years later than DNP and is based on polarisation transfer from the well-defined nuclear spin-singlet state of the two ^{1}H spins in the hydrogen molecule, which is called parahydrogen, to a target molecule. This can be achieved by the chemical involution of pH_2 to a target molecule by a hydrogenation reaction as was predicted in 1986 by Bowers and Weitekamp [3] and experimentally proven 1 year later [50,51]. Since these pioneering works, hyperpolarised substances generated via PHIP were used in various applications including: [52] the investigation of the kinetics of inorganic reactions; [53–55] to explore heterogeneous reactions; [56–58] the observation of the spatial distribution of hyperpolarised gases by MRI; [15,59] the use as contrast agent in MRI; [18,60–62] the transfer of the accomplished proton hyperpolarisation to hetero-nuclei using either suitable pulse sequences [63,64], adiabatic field cycling [65] or transport through level avoiding crossing; [27,66,67] the study of long-lived states [21,68,69] originating from pH_2 [24–26,70] and, far from chemical applications, the particular pH_2 spin state has been used in the context of quantum information processes [71–73]. In 2009, it was shown that temporary association of parahydrogen and a substrate on a transition metal-based catalyst is sufficient to transfer the polarisation to the substrate (signal amplification by reversible exchange, SABRE) [74,75]. This polarisation experiment can be applied to a significantly larger set of molecules as hydrogenative PHIP, as only a free electron pair is needed that can bind to the transition metal.

One major drawback for *in vivo* applications of DNP and PHIP is the necessary use of toxic substances, which are free radicals in the case of DNP and transition metal catalysts for PHIP. Furthermore, their presence in the sample enhances nuclear spin relaxation rates and limits the lifetime of the hyperpolarised state, an aspect especially important for *ex situ* applications. Therefore, a fast and reliable separation of radical/catalyst and

polarised substance is required. Different approaches for this separation were proposed in literature: One of them is the immobilisation of radicals in silica [42] or gel beads [76] in combination with a continuous flow setup, another one is the filtration of radicals using ion-exchange columns [9].

The chapter is organised as follows:

In Section 2, we present the application of two approaches to provide hyperpolarised and radical-free liquid for DNP-enhanced NMR and MRI. The first method is based on thermoresponsive, spin-labelled hydrophilic polymer networks (hydrogels), as a method for fast and simple separation of radicals and hyperpolarised sample. The second approach demonstrates continuous production of hyperpolarised water and MRI detection, using a mobile DNP polariser and a flow setup with nitroxide radicals immobilised on a sepharose gel matrix. Here, we show that the 180° phase shift of the hyperpolarised water can be used to generate a sufficient MRI contrast to distinguish hyperpolarised from thermally polarised water. In Section 3, we introduce methods for NMR spectroscopy and MRI for the optimal detection of ^{1}H PHIP signals which inherently exhibit an antiphase signal pattern. In Section 3.3, we demonstrate that the antiphase character of the PHIP signal can be used for selective detection of a small number of hyperpolarised protons in the presence of a large number of thermally polarised protons.

In Section 4, we address the problem of the short ^{1}H hyperpolarisation lifetime caused by relaxation processes. We show the possibility to store the hyperpolarisation in a nuclear spin-singlet state and analyse the methods to convert this MR invisible state into detectable magnetisation.

2. DYNAMIC NUCLEAR POLARISATION

2.1. DNP Theory

Detailed discussions of the theory of Overhauser DNP can be found in several papers and review articles [29–31,77,78], herein only a short summary will be given. Polarisation transfer with Overhauser DNP is based on the saturation of electron spin transitions with on-resonant MW irradiation. The second requirement is the presence of hyperfine coupling between unpaired electron spins and nuclear spins, which is fluctuating on a time scale on the order of the inverse electron spin Larmor frequency or faster. The steady-state signal enhancement E that can be obtained from Overhauser DNP is given by [29]:

$$E = 1 - \xi f s \frac{|\gamma_e|}{\gamma_n} \tag{4.1}$$

where γ_e and γ_n are the gyromagnetic ratios of the electron and nuclear spin, respectively. For nitroxide radicals and ^{1}H nuclei this ratio is $|\gamma_e|/\gamma_{1_H} \approx 659.4$. The coupling factor $\xi = -1 \ldots 0.5$ characterises the efficiency of the polarisation transfer and depends on the magnetic field, the nature of the hyperfine coupling, that is, dipolar, scalar or a combination of both, and the time scale on which the hyperfine interaction fluctuates. For ^{1}H Overhauser DNP with nitroxide free radicals in water at room temperature and 0.35 T, the coupling factor amounts to $\xi = 0.33 \pm 0.03$ [79–81]. The leakage factor $f = 0 \ldots 1$ gives the relative contribution of paramagnetic interactions to the total nuclear spin-lattice relaxation rate and, among others, depends on the radical concentration. The saturation factor s, describing the extent of the saturation of electron spin transitions, depends on the number of electron spin transitions and the MW power. The power dependence of the DNP enhancements can be written as [82]:

$$E(P) = 1 - (1 - E_{max}) \frac{P/P_{half}}{1 + P/P_{half}} \tag{4.2}$$

where E_{max} is the extrapolated enhancement in the limit of infinite MW power and the saturation parameter P_{half} is the MW power at which the saturation factor has reached 50% of its extrapolated value. For ^{14}N nitroxide radicals in low concentration or for ^{14}N nitroxide radicals attached to a matrix, continuous wave (CW) MW irradiation can basically saturate only one of the three electron spin transitions, which arise from intramolecular hyperfine coupling to the ^{14}N nucleus. Hence, in these systems the saturation factor is limited to $\lim_{P\to\infty} s = 1/3$ and the maximum obtainable enhancement for ^{1}H DNP is $\lim_{c\to\infty, P\to\infty} E(c, P) \approx -72 \pm 7$.

Due to the positive coupling factor, negative enhancements are observed for ^{1}H Overhauser DNP with nitroxide free radicals.

2.2. Thermoresponsive, Spin-Labelled Hydrogels as Separable DNP Polarising Agents

For many practical applications of DNP, it is necessary to remove free radicals from the hyperpolarised substance. On the one hand, *in vivo* applications may be hindered by the toxicity of the radicals. On the other hand, the lifetime of the hyperpolarised state, which is especially important for *ex situ* applications, is much shorter in presence of free radicals.

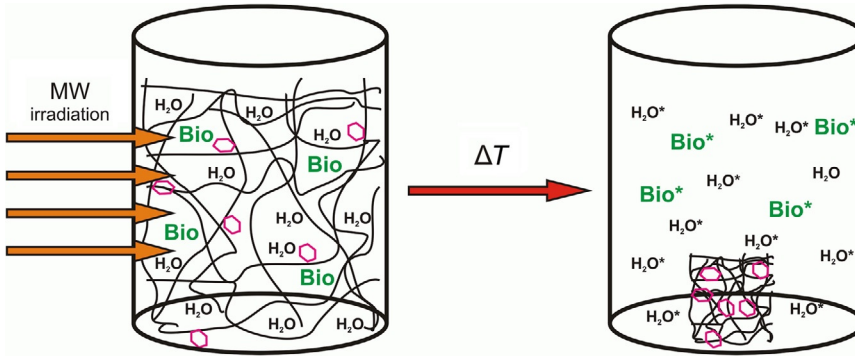

Figure 4.1 Scheme of DNP polarisation using a thermoresponsive spin-labelled hydrogel with a subsequent temperature-induced volume change resulting in the separation of radicals and hyperpolarised molecules (hexagon: spin-label, Bio: target biomolecules, * indicates the hyperpolarised state). *From Ref. [83]—Reproduced by permission of the PCCP Owner Societies.*

Thermoresponsive hydrogels [83] can be used for the separation of radicals and hyperpolarised substance, exploiting the collapse of the polymer network above the critical temperature T_C that results in a reversible and fast ($\leq$1 s) decrease of the volume by about 500%. During the polarisation process, electron spin transitions are saturated by MW irradiation, while at the same time dielectric losses result in an increasing sample temperature. Above T_C, the network starts to collapse, thereby expelling hyperpolarised liquid and target molecules and ending the polarisation process (Fig. 4.1).

In a former work [83], spin-labelled thermoresponsive hydrogels were synthesised with two different labelling degrees: SL-hydrogel-1 contains up to 5% of spin-labelled monomer units, resulting in a radical concentration of about 1 mM in the swollen state. Up to 15% of all monomer units are labelled in SL-hydrogel-2, corresponding to a radical concentration of about 6.8 mM in the swollen state. The details of the synthesis are given in Ref. [83]. The critical temperature of both hydrogels is $T_C = 63\,^{\circ}\mathrm{C}$ [84].

2.2.1 CW EPR

Figure 4.2 shows continuous wave electron paramagnetic resonance (CW EPR) spectra of both hydrogels and, for comparison, the CW EPR spectrum of a 10 mM aqueous solution of free TEMPOL radical (4-hydroxy-2,2,6,6-tetramethylpiperidine-1-oxyl). As a result of restricted motions of the immobilised radicals, linewidths for both hydrogels are significantly broader than those of the free radical. Moreover, rotational

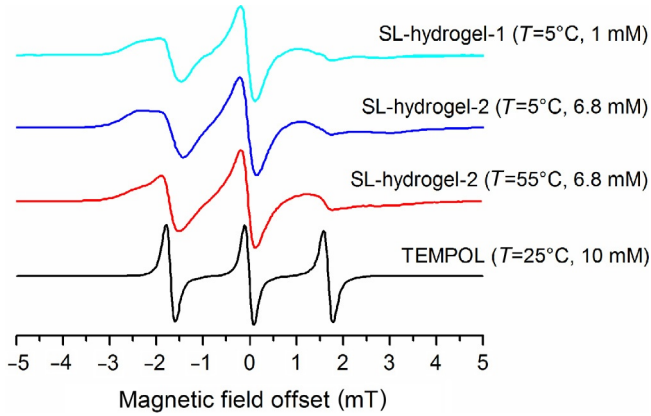

Figure 4.2 X-band CW EPR spectra of SL-hydrogel-1, SL-hydrogel-2 and for a 10 mM aqueous solution of the free nitroxide radical TEMPOL for comparison.

diffusion around the tether bonds, which connect the radical to the polymer backbone, is expected to be much faster than around the other directions. This anisotropy becomes manifest in the increased linewidth as well as in the additional features in the high- and low-field regions of the spectrum. Increasing the temperature to 55 °C resulted in larger rotational diffusion rates and therefore smaller anisotropic features. Comparing both hydrogels at 5 °C shows a slightly larger linewidth for SL-hydrogel-2, indicating stronger coupling among the unpaired electron spins.

2.2.2 ^{1}H Relaxation and DNP Enhancements

Proton spin-lattice relaxation times T_1 of water were measured in both labelled and unlabelled hydrogels and in pure water. Even in the unlabelled hydrogel (≈ 0.48 s), water showed a much shorter relaxation time than in the bulk (≈ 2.1 s). This indicates a reduced mobility of the water molecules in the hydrogel, which may result from the confinement of water molecules in the polymer network. As a result of the reduced mobility of both water and radical inside the hydrogel, DNP coupling factors in the hydrogel are expected to be smaller than for free radical in bulk water. For the labelled hydrogels SL-hydrogel-1 and -2, spin-lattice relaxation times of approximately 330 and 65 ms were found, respectively. Furthermore, relaxation times were found to depend sensitively on the swelling degree and the sample temperature, which are both not exactly known. Therefore, uncertainties for the T_1 measurements are as large as 20%. Leakage factors of $f = 0.31 \pm 0.20$ (SL-hydrogel-1) and $f = 0.86 \pm 0.04$ (SL-hydrogel-2) were obtained from T_1 measurements. Hence, DNP enhancements for

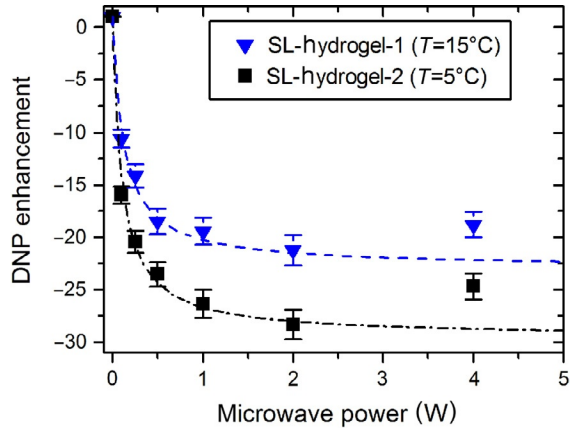

Figure 4.3 Measured DNP enhancements for various microwave powers (symbols) and fits of the power dependence according to Eq. (4.2) (line). The fit parameters are given in Table 4.1.

SL-hydrogel-1 are limited by the low leakage factor and larger enhancements are expected for SL-hydrogel-2.

Figure 4.3 shows DNP enhancements for varying MW power. During the experiments, the samples were cooled at 15 °C (SL-hydrogel-2) or 5 °C (SL-hydrogel-1). Maximum DNP enhancements of up to $E = -21.2 \pm 1.4$ and $E = -28.3 \pm 1.4$ were obtained at a MW power of 2 W for SL-hydrogel-1 and SL-hydrogel-2, respectively. In general, dielectric sample heating increases the sample temperature depending on the MW irradiation time and power. For MW power exceeding 2 W, these heating effects cause the polymer network to collapse before steady-state polarisation is reached, resulting in lower DNP enhancements. Furthermore, if sample heating results only in a partial collapse of the hydrogel network, expelling only a part of the water from the network, the remaining water is subject to further reduced mobility in the shrunken gel and therefore exhibits a lower coupling factor than in the completely swollen gel.

MW power-dependent DNP enhancements were fitted using Eq. (4.2). The resulting fits are shown as lines in Fig. 4.3 and the fitting parameters $E_{\max}$ and P_{half} are given in Table 4.1. Due to difficulties in separating the saturation factor s and coupling factor ξ for our system, we report the product $\xi \cdot s$ as determined from the maximum measured enhancement E using Eq. (4.1) and the calculated leakage factor f.

As a result of the larger labelling degree of SL-hydrogel-2, that results in a larger leakage factor, both measured and extrapolated DNP enhancements

Table 4.1 DNP parameters for SL-hydrogel-1 at 15 °C and SL-hydrogel-2 at 5 °C

	SL-hydrogel-1	SL-hydrogel-2
Labeling degree (%)	5	15
Estimated concentration (mM)	1.0 ± 0.2	6.8 ± 0.5
E_{max}	-22.9 ± 1.2	-29.4 ± 1.5
E	-21.2 ± 1.4	-28.3 ± 1.4
P_{half} (W)	0.12 ± 0.03	0.10 ± 0.02
f	0.31 ± 0.20	0.86 ± 0.04
$\xi \cdot s(P = 2\ \mathrm{W})$	0.109 ± 0.070	0.049 ± 0.003

were larger for SL-hydrogel-2. However, the difference in $\xi \cdot s$ indicates a lower coupling factor or saturation factor for the latter. Since ξ is expected to be independent of the labelling degree, this difference may be attributed to the lower temperature for SL-hydrogel-2, resulting in lower water mobility compared to SL-hydrogel-1 at 15 °C and therefore in a lower coupling factor.

While the thermal collapse of the polymer network limits the achievable DNP enhancements, it enables hyperpolarisation and separation of hyperpolarised liquid from toxic radicals in a single step. Furthermore, the separation of the hyperpolarised molecules increases the nuclear spin-lattice relaxation time and therefore the lifetime of the hyperpolarised state. A spin-lattice relaxation time of $T_1 \approx 2100$ ms at 25 °C was measured in water expelled from the hydrogel. The absence of spin labels in the expelled water was verified by CW EPR, showing no signal indicative of radicals (data not shown).

2.2.3 Temperatur Dependence of DNP Enhancements

Figure 4.4 shows DNP enhancement measured for both hydrogels at 2 W for various cooling temperatures, showing that largest enhancements were obtained for lower temperatures (5–25 °C). At higher temperatures, the partial collapse of the hydrogel network limited the hyperpolarisation process, therefore reducing DNP enhancements. This is in contrast to systems without thermoresponsivity, where the coupling factor and, hence, the DNP enhancement increase with temperature due to a higher mobility of both water molecules and radicals. From the monotonically and smoothly decreasing enhancements, especially for SL-hydrogel-2, we conclude that even at low temperatures and 2 W MW power, a partial collapse of the

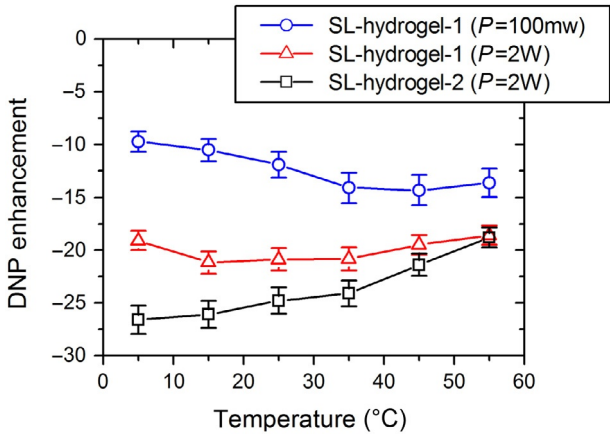

Figure 4.4 Temperature dependence of the DNP enhancement for both hydrogels at 2 W microwave power and for SL-hydrogel-1 at 100 mW microwave power.

hydrogel network limited DNP enhancements. This is in agreement with a study by Junk *et al.* [85], where it was shown that the thermally induced collapse on the molecular scale proceeds over a substantially broader temperature range than indicated by the sharp macroscopic volume transition at T_C.

When MW power was reduced to 100 mW, which is small enough to avoid substantial sample heating and therefore the heating-induced collapse, larger DNP enhancement were observed for increasing temperature due to an increasing coupling factor. However, for temperatures approaching T_C, DNP enhancements did not increase further, indicating that already at these temperatures the thermoresponsivity of the hydrogel affects the polarisation process.

Hence, two opposing effects have to be considered to optimise the enhancement factor. On the one hand, the DNP coupling factor increases with higher temperature due to increased mobility. On the other hand, the collapse of the hydrogel network induced by MW heating separates the spin labels and target molecules, resulting in lower enhancements.

We have shown that hyperpolarisation of water by DNP as well as the separation from radicals can be performed in a single step by making use of the collapse of a spin-labelled hydrogel network at elevated temperatures. These unique properties suggest the use of the studied system as a polarising agent for both *in situ* and *ex situ* DNP experiments. For *in situ* experiments, this system can avoid line broadening effects and enhanced spin-lattice relaxation that normally would result from the presence of a paramagnetic radical in the solution. For *ex situ* experiments, the greatest benefit is the prolonged

lifetime of the hyperpolarised state during the transport time. Furthermore, these properties suggest the use of SL-hydrogels for dissolution DNP, providing a radical-free and non-toxic solute after the dissolution step.

2.3. Flow DNP-Enhanced MRI Using Radicals Immobilised on Sepharose Beads

Another approach to separate the radical from the hyperpolarised liquid is the use of a flow system. [9,17,86] To explore applications of the flow system approach for the production of hyperpolarised water, we added a pump system to a mobile DNP setup based on a Halbach magnet [17,87,88] to perform DNP experiments at flow conditions. The Halbach system is constructed from permanent iron neodymium boron alloy magnets and can be tuned to a magnetic field of 0.35 T [89]. The use of a Halbach system is beneficial with regard to medical applications, since it has nearly zero-stray field outside and can be brought close to an MRI scanner [17].

Figure 4.5 shows a sketch of the flow experiment as similarly reported by Han *et al.* [43] and based on the pioneering work of Dorn *et al.* [90]. A reservoir provides pure water, which is pumped through a Halbach magnet, in which it initially builds up thermal polarisation. The tube used for the flow system has an inner diameter of approximately 1 mm. In the Halbach magnet, NMR and DNP experiments are performed using an ENDOR (electron nuclear double resonance) probehead. Within this probehead, the flow tube is placed, in which the water is in contact to a 4-amino-TEMPO

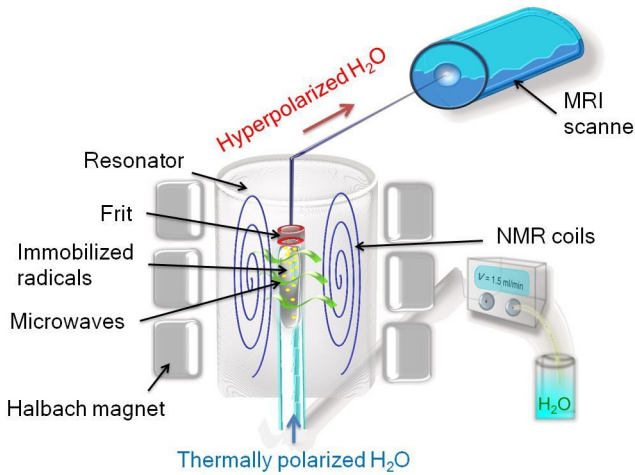

Figure 4.5 Sketch of the flow system.

(4-amino-2,2,6,6-tetramethylpiperidine-1-oxyl) labelled Sepharose matrix. At this position, MWs with a frequency of around 9.7 GHz are irradiated, corresponding to the electron spin Larmor frequency at 0.35 T. A frit prevents the Sepharose from flowing out of the cavity of the ENDOR probehead.

Thereby, the radicals are removed from the liquid, which is not only favourable in terms of medical applications but also for microfluidic applications [91]. The Halbach magnet is placed in front of an MRI scanner in order to shorten the distance between the point of hyperpolarisation and *ex situ* detection, therefore minimising the effect of T_1 relaxation, which reduces the detectable hyperpolarised signal in the MRI scanner. To further decrease the transfer time between Halbach magnet and MRI scanner, a tube of 150 μm inner diameter is used after the frit. Exploiting Bernoulli's principle, that is, the inverse proportionality of the average flow velocity and the square of the radius, one can reduce the time between hyperpolarisation in the Halbach magnet and detection in the MRI scanner by a factor of approximately 13. Eventually, we are able to perform NMR spectroscopy and imaging on the hyperpolarised water in the MRI scanner.

2.3.1 Measurements at 0.35 T

To compare the performance of the spin-labelled Sepharose to free TEMPOL, we measured the negative enhancement in dependence of the applied flow rate, see Fig. 4.6. For all measurements, the tube used has an inner diameter of 1 mm.

For all experiments, the irradiation time was 2 s. The effective irradiation time of the sample depends on the flow velocity. As a consequence, higher flow rates will lead to a lower hyperpolarisation build-up. However, the initial residence time in the magnet and therefore the effective enhancement is also influenced by the different thermal polarisation build-up at different flow rates. Depicting all effects which influence the enhancement is therefore complex and some parameters are not readily accessible. For instance, the Sepharose matrix is effectively reducing the inner diameter of the tube inside the cavity, which in turn leads to an increased average flow velocity and therefore a shortened residence time inside the irradiated volume.

2.3.2 Measurements at 4.7 T

After hyperpolarisation, the water is pumped to the MRI scanner for spectroscopy and imaging. Even for the highest flow rates of 1.5 ml/min it takes about 1.5 s to transfer the water from the Halbach magnet to the MRI scanner. In case of free TEMPOL dissolved in water, this time is on the order of

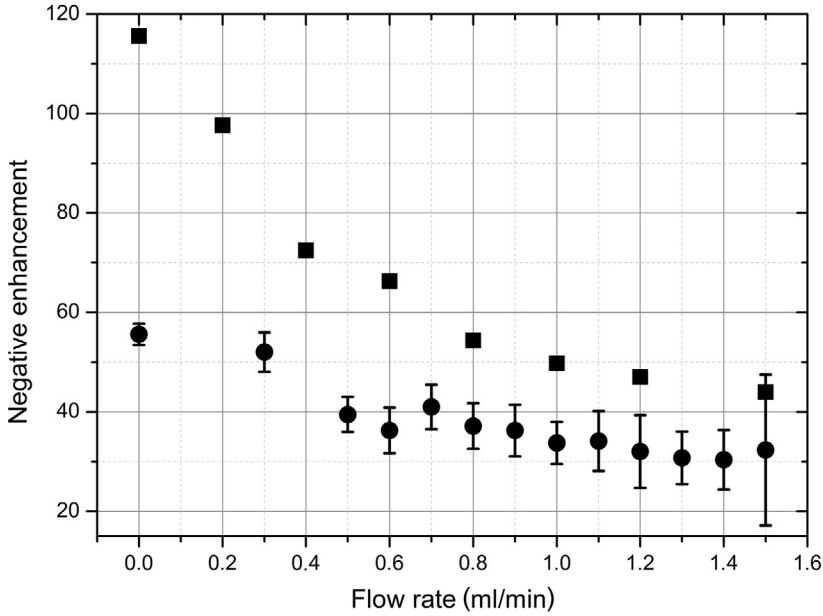

Figure 4.6 Negative enhancements of spin-labelled Sepharose and free TEMPOL, measured for different flow rates in the Halbach magnet. *From Ref. [17]—Reproduced with permission of Springer-Verlag, Berlin.*

$4T_1$. Hence, almost no enhancement is expected in this case. In the case of the spin-labelled Sepharose, the relevant relaxation time is the one of pure water after passing the gel matrix, since no free radicals are present in the liquid.

The obtained DNP enhancement in the MRI scanner is shown in Fig. 4.7. In contrast to the measurements at 0.35 T in the Halbach magnet, the tube diameter in the NMR coil is 150 µm. Like expected, almost no enhancement is observed for free TEMPOL in water. For all flow rates, the signal after hyperpolarisation is close to the reference measurement. This is due to the fast T_1 relaxation time, as mentioned above. In contrast to that, the obtained enhancement in case of the spin-labelled Sepharose is increasing with increasing flow rates. Dorn *et al.* derived a formula to describe the observed *ex situ* enhancement after *in situ* hyperpolarisation [92]:

$$E_{\text{obs}} = \frac{E}{K} \cdot \left(1 - \mathrm{e}^{-\frac{t_\mathrm{a}}{T_{1\mathrm{a}}}}\right) \cdot \mathrm{e}^{-\frac{t_\mathrm{b}}{T_{1\mathrm{b}}}} \cdot \mathrm{e}^{-\frac{t_\mathrm{c}}{T_{1\mathrm{c}}}} \tag{4.3}$$

here $\exp(-t_\mathrm{a}/T_{1\mathrm{a}})$ describes the hyperpolarisation build-up in the Halbach magnet and $\exp(-t_\mathrm{b}/T_{1\mathrm{b}})$ and $\exp(-t_\mathrm{c}/T_{1\mathrm{c}})$ describe the hyperpolarisation

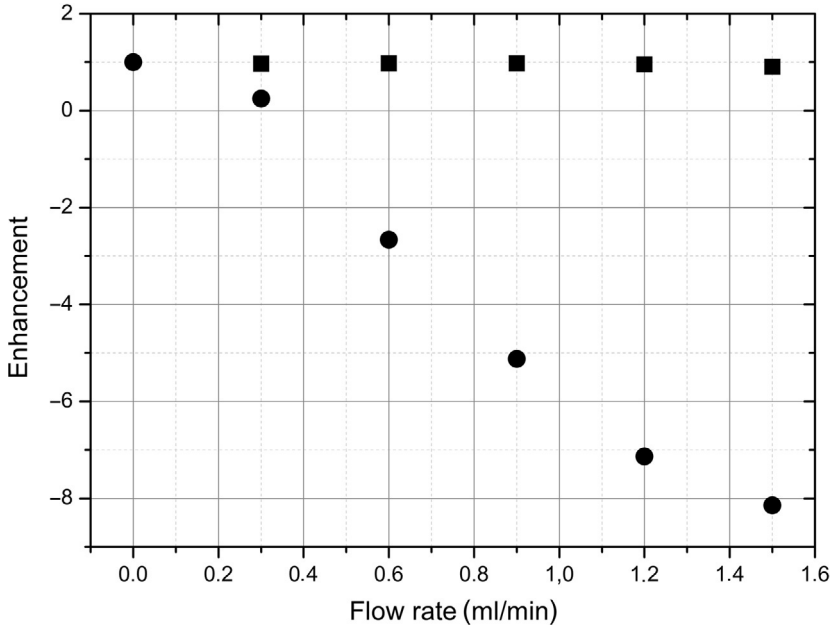

Figure 4.7 DNP enhancement for different flow rates recorded in the MRI scanner for 5 mM TEMPOL (closed square) and spin-labelled Sepharose (closed circle). *From Ref. [17]—Reproduced with permission of Springer-Verlag, Berlin.*

decay in the region between the Halbach magnet and the MRI scanner and within the MRI scanner, respectively. The constant K, which is the ratio of the magnetic fields in the high- and low-field region, takes into account the difference in thermal polarisation and E is the initial enhancement, as measured in the Halbach magnet. The formula shows that the observed enhancement depends not only on the ratio of the different fields, but also on the different hyperpolarisation build-up and decay times. Though it is possible to calculate the enhancement, we aim at a more general explanation. The reason is that T_{1b} is time dependent due to the different stray fields experienced by the sample during the transport between Halbach magnet and MRI scanner.

Several aspects affect the enhancement measured in the MRI scanner as shown in Fig. 4.8: First, the hyperpolarised substance is transported faster to the MRI scanner at higher flow rates and, hence, experiences smaller losses due to spin-lattice relaxation. However, at the same time the hyperpolarisation build-up in the Halbach magnet is decreasing, because of a decreasing residence time in the ENDOR probehead. In addition, the

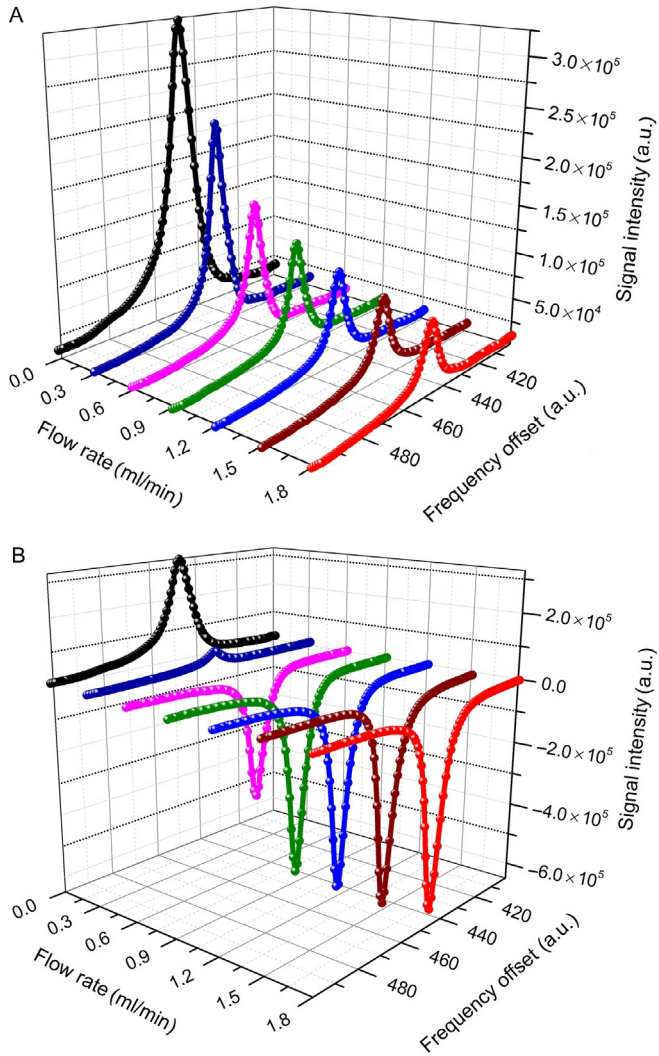

Figure 4.8 Measured reference (A) and hyperpolarised (B) signal at the MRI scanner for different flow rates.

thermal reference signal decreases at higher flow rates since shorter residence times in the magnet limit the built-up of thermal polarisation.

Figure 4.8 shows how the hyperpolarisation is evolving with increasing flow rate. For a flow rate of 0.3 ml/min, the hyperpolarised signal is diminished in comparison to the reference due to the negative enhancement for ^{1}H Overhauser DNP. This flow rate is just high enough to transport some of

the hyperpolarisation, but not sufficient to invert the signal. The first time one can observe signal inversion is at 0.6 ml/min. After that the hyperpolarised signal reaches a plateau where it does not significantly change anymore with increasing flow rate. Hence, we conclude that further increases in the enhancement result from a decreasing reference signal rather than an increasing hyperpolarised signal. Again some parameters are counterbalancing each other, like incomplete hyperpolarisation in the Halbach magnet and decreasing transport time to the MRI scanner.

2.3.3 Imaging at 4.7 T

In order to explore the capabilities of hyperpolarised water as MRI contrast agent, several images were recorded. For hyperpolarised imaging we used tubes of 700 and 1800 μm diameter, respectively. The raw data were four times zero filled prior to Fourier transformation. The images acquired in a 700 μm tube are shown in Fig. 4.9, showing a two times larger DNP signal as compared to the thermal reference signal. However, the enhancement is significantly lower than for the 150 μm tube, which is a result of the reduced flow velocity in the tube, leading to stronger T_1 relaxation of the hyperpolarisation.

To further investigate the hyperpolarisation decay within the tube, we adapted an even bigger tube of 1.8 mm inner diameter (Fig. 4.10).

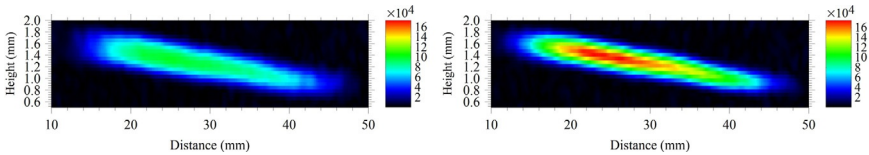

Figure 4.9 Left: Image of thermal signal in a 700-μm tube in the MRI scanner. Right: hyperpolarised signal. *From Ref. [17]—Reproduced with permission of Springer-Verlag, Berlin.*

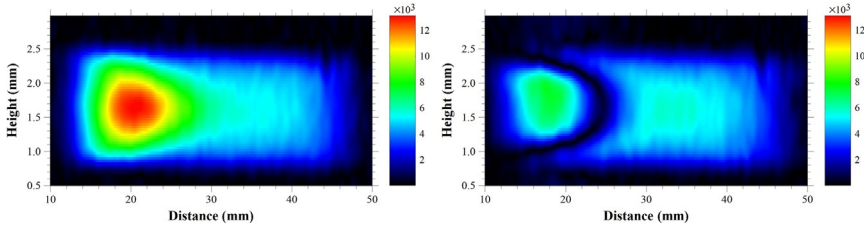

Figure 4.10 Left: image of thermal signal in a 1.8-mm tube in the MRI scanner. Right: hyperpolarised signal. *From Ref. [17]—Reproduced with permission of Springer-Verlag, Berlin.*

Now the velocity is reduced further and the magnitude of the thermal signal is higher than the hyperpolarised signal, which again results from a stronger hyperpolarisation relaxation and the inverted signal. Additionally, a region of zero intensity shows up. To understand where the region of zero intensity in the case of the hyperpolarised signal comes from, it is helpful to look at the phase map: Fig. 4.11 shows a 180° phase shift in the region with hyperpolarised signal due to the negative DNP enhancement, corresponding to the area before the zero crossing in Fig. 4.10.

In Fig. 4.12, a one-dimensional cross-section of the images in Figs. 4.10 and 4.11 is given, showing that the point of zero intensity falls together with the point where the phase shift drops from 180° to zero. In the hyperpolarised region the signal is inverted, as can be told from the phase

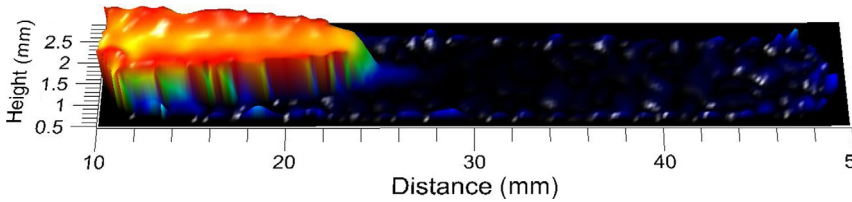

Figure 4.11 Phase map for Fig. 4.10. The phase shift of the hyperpolarised signal relative to the thermal signal is given by the plateau and corresponds to 180°.

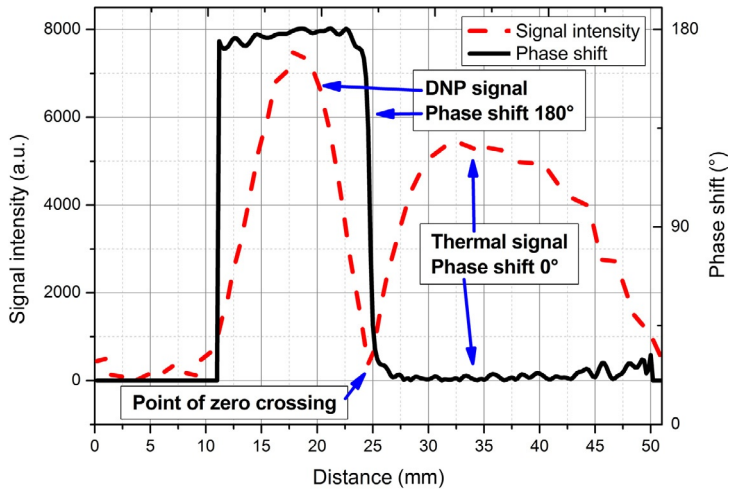

Figure 4.12 One line in the axial direction of the hyperpolarised signal of Fig. 4.10 (dashed) and the corresponding line of the phase map (straight), dependent of the pumped distance within the tube.

map, again with a smaller intensity than the thermal reference signal. Within the tube and because of the slow flow velocity, the hyperpolarised signal relaxes to thermal equilibrium. As the hyperpolarised liquid has travelled a certain distance, for example, around 25 mm in Fig. 4.12, the hyperpolarisation has decayed due to spin-lattice relaxation but the thermal polarisation has not yet built-up. Therefore, the total signal is zero at this position. After this point of zero crossing, the signal is increasing towards thermal equilibrium, which leads to a phase shift of zero for the rest of the distance. The 180° phase shift therefore provides valuable additional information, especially in case of small enhancements.

We have shown that the mobile DNP setup based on a Halbach magnet is a useful and flexible alternative to, for example, electromagnets. We are able to provide hyperpolarised and radical-free water for *ex situ* detection. In addition we have shown that the phase shift that results from negative DNP enhancements is very useful, since it gives an excellent MRI contrast when detected in a phase sensitive manner.

3. PARAHYDROGEN-INDUCED POLARISATION

3.1. Introduction

An alternative method beside DNP to achieve a nuclear alignment is PHIP. In the pioneering works by Bowers and Weitekamp [3,50] and Eisenschmid *et al.* [51], they showed that this method is based on the spin order transfer of pH_2 to an unsaturated molecule by a hydrogenation reaction. Twenty years later, it was shown that the spin order of the two parahydrogen atoms attached to a transition metal catalyst can be transferred to the ligand system of the catalyst. Chemical exchange with free ligand molecules in the solvent results in hyperpolarised dissolved molecules, thereby overcoming the classical restriction of the PHIP technique to unsaturated molecules [74,75]. This method is called SABRE. However, it is beyond the scope of this contribution where we solely discuss PHIP experiments which achieve hyperpolarisation by a homogeneously catalysed hydrogenation of unsaturated substrates.

Parahydrogen is the spin-singlet isomer of the two ^1H spins in molecular hydrogen. It has a total nuclear spin of zero and is therefore invisible in NMR experiments. Since protons are Fermions, the wavefunction of the hydrogen molecule has to be antisymmetric in exchange of the nuclei. This condition can only be fulfilled by the product of the molecular rotational angular momentum and the nuclear spin angular momentum. Hence,

pH_2 exists only in the even rotational states whereas the spin triplet isomer orthohydrogen only in the odd rotational states. By cooling hydrogen in the presence of active charcoal, parahydrogen can be enriched (e.g. to 93% at 35 K). Herein, active charcoal allows the system to reach the thermodynamical equilibrium within minutes. Since the conversion of para- to orthohydrogen in the absence of active charcoal is very slow, the enriched parahydrogen can be stored at room temperature for several days.

Hyperpolarisation can be achieved by the hydrogenation of an unsaturated molecule with pH_2 [5,93]. For this purpose, a catalyst is required which transfers pairwise and simultaneously the two parahydrogen protons while keeping their relative spin orientation. Pictorially described, this results in a hyperpolarisation since only Zeeman energy levels in the product molecule become populated which fulfil the antisymmetric spin orientation of the former pH_2 protons. Two experimental procedures in PHIP experiments are distinguished which are called PASADENA [50,51] and ALTADENA [94]. In the PASADENA experiment, the hydrogenation is performed inside the high magnetic field of the NMR spectrometer in which the two former pH_2 protons are weakly coupled in the product molecule. In contrast, in the ALTADENA experiment, the hydrogenation takes place in a low magnetic field where the protons are strongly coupled and the sample is subsequently transported into the spectrometer. The resulting density operators of the two experiments differ significantly. However, in contrast to the thermal polarisation, they both contain two-spin order terms like $I_z^1 I_z^2$. A thorough theoretical introduction can be found in Ref. [52].

These two-spin order terms lead to a special behaviour of the spin system in spectroscopy or imaging experiments. For example, they result in antiphase signal contributions in the NMR spectra which are in the case of the PASADENA experiment only separated by the J-coupling (Fig. 4.13). Therefore, linewidth broadening by magnetic field inhomogeneities can cause partial signal cancellations of the antiphase contributions. This problem is addressed in Section 3.2. In Section 3.3, the characteristics of PHIP hyperpolarised spin states under ^{1}H imaging sequences are analysed with a special focus on the sequence echo time TE.

3.2. Avoiding Signal Cancellations in PHIP Spectroscopy

In this section, we will address the problem of acquiring a well-resolved multiplet (or multiplets) arising from a PHIP experiment in inhomogeneous magnetic fields. The inhomogeneity might result from an inhomogeneous

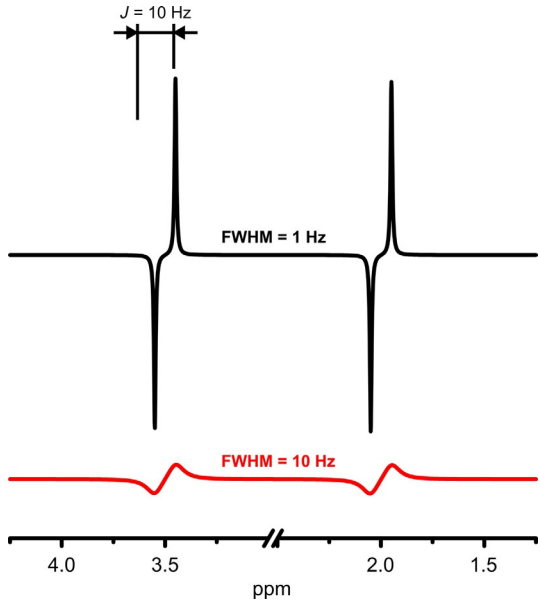

Figure 4.13 Two simulated PASADENA spectra for an *AX* spin system, with different linewidths. When the FWHM of the Lorentzian is on the order of the J-coupling constant, the majority of the signal is lost due to cancellation.

B_0 itself or is induced by the presence of elements that perturb the polarising field. Let us consider first, and with no loss of generality, that both hydrogen nuclei from pH_2 (labelled as 1 and 2) occupy two chemically inequivalent sites once the hydrogenation reaction has finished. Furthermore, we assume that they form an isolated AX spin system [95], that is, their chemical shift differ in a number much larger than their indirect coupling constant J_{12}. If the reaction takes place at the same (high) magnetic field where the NMR experiments are performed (PASADENA), the resulting spectrum presents two antiphase doublets with a splitting equal to their coupling constant. In contrast, if the system is at thermal equilibrium before the NMR experiment, two in-phase doublets (with the same splitting value) are observed in the spectrum. The presence of antiphase doublets in PASADENA comes from the special form of the density operator after the hydrogenation with parahydrogen, more precisely with the part including a longitudinal two-spin order term of the form $I_z^1 I_z^2$ [93,96].

The difference between the initial density operator in either PHIP or thermally polarised samples becomes very important when the magnetic field homogeneity is limited. The homonuclear coupling constants, J_{H-H},

are of the order of few Hz in liquid samples, thus even tiny perturbances in the homogeneous magnetic field produce partial signal cancellation of the antiphase signals. There are mainly two sources of line broadening: the intrinsic inhomogeneity of the external magnetic field and the susceptibility changes produced by the sample or by the experimental setup. This imposes limitations in the large variety of experiments in which the hyperpolarisation obtained by PHIP can be used.

In particular, PASADENA experiments are more sensitive to line broadening, because the presence of an extra term related to the polarisation difference $(I_z^1 - I_z^2)$ in an AX two-spin system tends to prevent the signal cancellation in ALTADENA experiments. To illustrate the sensitivity of PASADENA to the magnetic field homogeneity, we present in Fig. 4.13 a simulation of two spectra of an AX system with $J_{12} = 10$ Hz. If the B_0 homogeneity is such that the peaks have a characteristic linewidth of 1 Hz, no signal loss occurs whereas if the inhomogeneity is increased to produce a spectrum with 10 Hz linewidth, the peak integrals are significantly smaller [97]. On one hand, we produced hyperpolarisation, but on the other hand, we lose it due to magnetic field inhomogeneities. This limits the applicability of PHIP in NMR spectroscopy to small volume samples and highly homogeneous B_0 fields.

3.2.1 Partial J-Spectroscopy

Our approach to tackle the problem of inhomogeneity is based on J-spectroscopy, a concept introduced by Allerhand in the 1960s [98]. In short, when a CPMG sequence is applied to a coupled spin system (in liquid state) the top of the successive echoes appear to be modulated. In particular, if all chemical shift differences are much larger than the couplings, and the echo time is chosen large enough to allow the smallest chemical shift to evolve, the evolutions with the Hamiltonian linear on the spins, $H = \sum_i a_i I_z^i$, such as chemical shift or inhomogeneities effects are refocused at the top of the echoes. On the other hand, evolutions with the Hamiltonians bilinear on the spins, $H = \sum_{i,j} b_{ij} I_z^i I_z^j$, such as J-coupling evolutions, are unaffected by refocusing 180° pulses [95,99]. If the signal at the top of those echoes is collected, the obtained pseudo-FID displays only information about J-coupling [100]. After a Fourier transformation the data result in a J-spectrum essentially free of inhomogeneity effects, where the linewidth is now related to $(\pi T_2)^{-1}$ instead to $(\pi T_2^*)^{-1}$. This situation is depicted in the left panel of Fig. 4.14, where the multiplets collapsing at zero frequency with much smaller linewidths are shown.

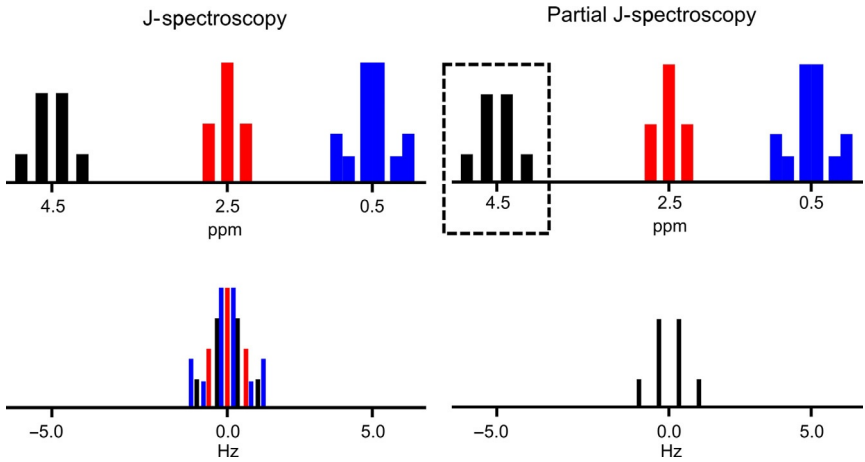

Figure 4.14 J-spectroscopy (left panel) and partial J-spectroscopy (right panel).

More technically speaking, if the following conditions are satisfied the resonance lines will only be related to the coupling constant:

(1) B_0 must be strong enough to ensure first-order approximation for the couplings, that is, weak coupling limit [95],

(2) the separation of the refocusing pulses must be large to ensure the free evolution under the smallest chemical shift difference of at least one period,

(3) the refocusing pulses must be carefully adjusted,

(4) any extra source of modulation must be absent.

If one or few of these conditions are not satisfied, the resulting multiplets will display different anomalies. If the spin system is strongly coupled or the refocusing pulses are not set accurately, new frequencies will be present in the echo-train envelope, related to the chemical shifts. If the echo time is too long, the resonance positions are shifted, whereas if it is too short, all J-modulations will disappear. In any of these cases, the spectrum obtained from the echo train is called spin-echo spectrum instead of a J-spectrum [101].

Even if all conditions are fulfilled, the J-spectra can become very complex if the sample presents several multiplets, as can be seen in the Fig. 4.14. If all information appears in a small frequency region, the interpretation of the J-spectrum might be cumbersome. In 1971, Ray Freeman and coworkers [101] presented an elegant idea to overcome this issue, consisting in the acquisition of the top of the echoes with a digital filter which filters out all undesired frequencies (see right panel of Fig. 4.14). This results in a highly

resolved multiplet facilitating a thorough interpretation. By simply moving the filter, it is possible to reconstruct the whole spectrum. The authors suggested in their paper to refer to this filtered data as partial J-spectrum.

3.2.2 CPMG Sequence Modified for PASADENA

Before implementing partial J-Spectroscopy for PASADENA, some modifications of the CPMG sequence had to be introduced. Firstly, the exciting 90° pulse is replaced by a 45° pulse, which produces maximum signal when the initial density operator is proportional to a longitudinal two-spin order. In fact, 90° pulses produce exactly zero signal in this situation. Secondly, a change related to the chemical reaction is mandatory: although it is not impossible [102], it is very difficult to exactly reproduce the results of the chemical reaction prior to each acquisition; therefore a single-scan acquisition is desired. However, as the CPMG sequence is very sensitive to imperfect pulses a proper phase cycling is usually performed which requires more than one scan. Alternatively, we have changed the phases of the pulses in the same scan to obtain $90_y - (180_x - 180_x - 180_{\bar{x}} - 180_{\bar{x}})_n$ as suggested by Guillon *et al.* [103]. The pulse sequence with the modifications is shown in Fig. 4.15.

3.2.3 Acquisition of a Highly Resolved Multiplet with Hyperpolarised 1-Hexene

In order to test the modified CPMG pulse sequence, we have selected the hydrogenation of 1-hexyne with parahydrogen which produces hyperpolarised 1-hexene. The complexity of the J-coupling network of 1-hexene makes it a challenging system. The reaction is depicted in Fig. 4.16. The experiments were carried out at 300 MHz Larmor frequency, where the former pH_2 protons labelled as H_A and H_B are weakly coupled to each other. Additionally, the proton H_B is strongly coupled to H_C at this

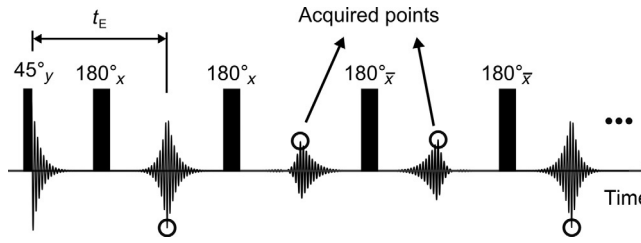

Figure 4.15 CPMG pulse sequence modified for PASADENA experiments.

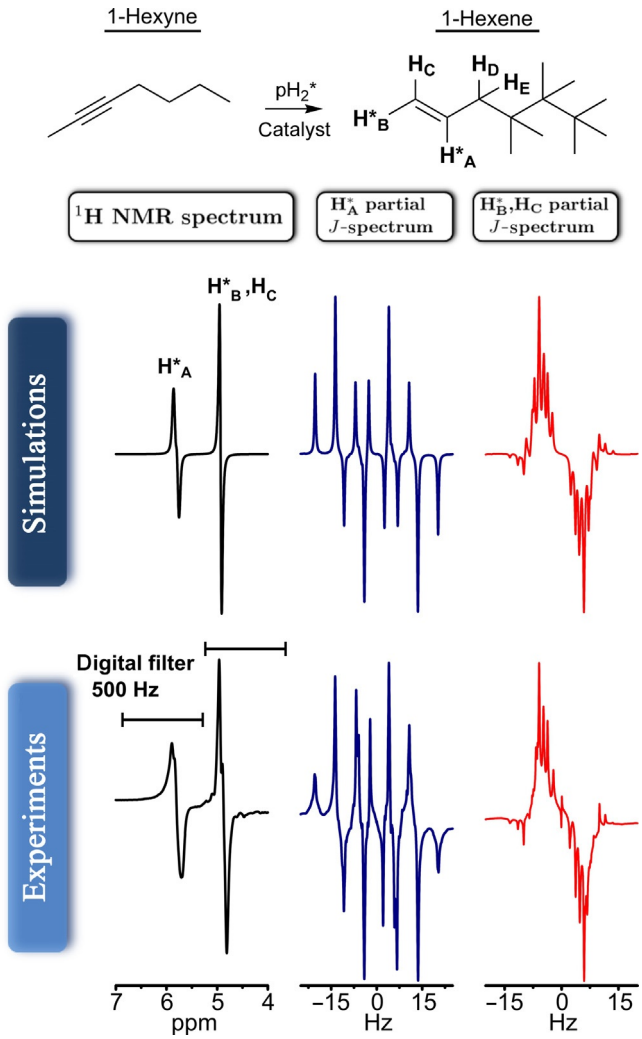

Figure 4.16 Hydrogenation reaction shown schematically with simulated and experimental results obtained with the pulse sequence depicted in Figure 4.15.

magnetic field strength, and both H_A and H_B are coupled to H_D and H_E with a relatively large coupling value (for more details see Ref. [97]).

Numerical simulations including these five spins were performed and compared with the experimental results. In Fig. 4.16, simulations of the hyperpolarised PASADENA NMR spectrum as well as the partial J-spectra centred at the frequencies of the former pH_2 protons are displayed along with the corresponding experimental results. To match the linewidths

obtained in the experiments, Lorentzian distribution of frequencies with FWHM = 15 and 0.5 Hz, respectively, were used for the calculation of the spectrum and the partial J-spectra. The echo time was set to TE = 8 ms and the position and width of the digital filter are indicated in the measured NMR spectrum. The excellent agreement between calculations and experiments demonstrates the good performance of the sequence and its ability to remove line broadening produced by magnetic field inhomogeneities.

3.3. ^{1}H MR Imaging with Substances Hyperpolarised via PHIP

As we discussed in detail in Section 3.2.3, hyperpolarisation achieved by PHIP gives rise to antiphase ^{1}H NMR signals. Thus, an old concern for the usage of PHIP in ^{1}H MRI was that the hyperpolarised signal cannot be detected in MR images because the antiphase signals might cancel each other in an imaging voxel. Due to this and due to the fast T_1 relaxation of protons, MRI of PHIP polarised substances was usually accomplished after transfer of the ^{1}H hyperpolarisation to ^{13}C [60,104]. Using ^{13}C for MRI applications has the additional advantage of negligible background signal as the natural abundance of ^{13}C in the body is very low. Thus, exciting medical applications of hyperpolarised ^{13}C MRI have been realised in recent years, the most prominent one being metabolic MRI to improve tumour diagnosis [10,11,13]. However, in this section, we will demonstrate that also ^{1}H PHIP MRI can be accomplished by a simple variation of a standard imaging sequence [18]. Moreover, the different temporal evolution of the PHIP signal compared to a thermal signal can be used to generate an excellent MRI contrast of a small amount of hyperpolarised protons to a large thermal background signal as it would be the case for *in vivo* applications.

Simply speaking, the antiphase character of the PHIP signal and thus its difference to thermal polarisation manifests itself in the temporal evolution of the spin system after an rf pulse, as can be seen in the FIDs depicted in Fig. 4.17. Our phantom for this experiment consisted of a 10 mm tube containing the PHIP substance (1-hexyne in deuterated acetone with PHIP catalyst; for details please refer to Ref. [18]) placed in the centre of a 30 mm tube containing a large volume of pure water. All experiments were performed in a standard 1.5 T clinical MRI tomograph. The bottom FID in Fig. 4.17 corresponds to the FID of the whole phantom in the thermally polarised case and is dominated by the exponential T_2^* decay of the water signal due to the large number of water protons being present in the sample. The top FID was acquired when the centre tube of the phantom contained

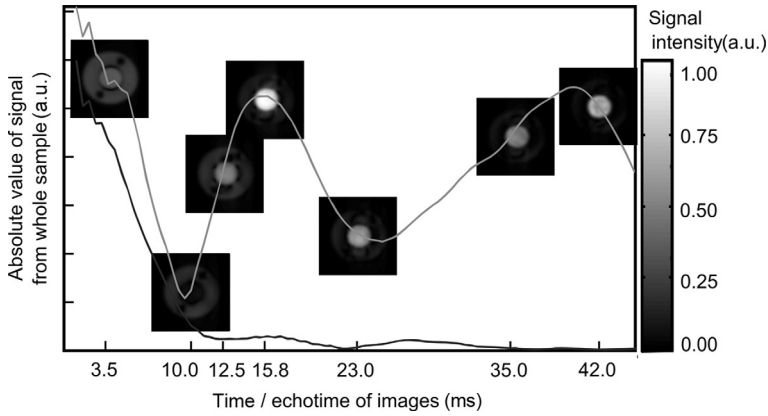

Figure 4.17 FIDs and MR images originating from a phantom consisting of two concentric tubes. The inner (10 mm diameter) tube contains the hyperpolarisation mixture whereas the outer tube (30 mm diameter) contains normal water. The bottom FID stems from thermally polarised water and the thermally polarised PHIP substance. The top FID is generated by thermally polarised water and the hyperpolarised PHIP substance exhibiting an antiphase NMR signal. The MR images were acquired with different echo times and overlaid on the hyperpolarised FID. Imaging was performed by using a gradient echo sequence with centric reordering and the following parameters: flip angle: 10°, repetition time: 45 ms, bandwidth: 600 Hz, FOV: 50 mm^2, resolution: 0.7 mm/pixel and total acquisition time: 3.96 s.

hyperpolarised 1-hexene and shows major signal oscillations due to the J-coupling of the hyperpolarised protons. Note that due to the fast T_2^* relaxation in the thermally polarised case, the thermal signal has almost completely decayed when the hyperpolarised signal reaches the first maximum due to the J-coupling induced refocusing of the PHIP antiphase signal.

These different time evolutions of the hyperpolarised versus the thermally polarised signal can be easily used to generate an excellent ^{1}H MRI contrast when the echo time of the MRI sequence is optimised for the acquisition of the refocused PHIP signal. The images overlaid on the hyperpolarised FID in Fig. 4.17 were acquired using a standard gradient echo MRI sequence with varying echo times. Figure 4.17 clearly shows that the intensities of the thermally and hyperpolarised regions of the images at different refocusing times (in the MRI sequence equal to the echo time TE) exactly follow the temporal evolution of the corresponding FIDs. For the water region (outer area) of the phantom, the signal intensity is maximal for the shortest refocusing time. In contrast, the image intensity of the PHIP area is low in the beginning and shows two pronounced maxima for 15 and

42 ms. As the signal of the water region almost completely decays within 10 ms, the PHIP images acquired at the maxima of the FID show excellent contrast to the thermally polarised background. These experiments verify that simply varying a delay of the MRI sequence is sufficient to generate outstanding contrast between a small amount of hyperpolarised protons and a large background signal.

Our results may open up unprecedented opportunities to use the standard MRI nucleus ^{1}H, for example, for metabolic imaging in the future which would significantly reduce the technical demands that arises from MRI of hetero-nuclei (e.g. broadband amplifiers and coils). Moreover, most hetero-nuclei (especially ^{13}C and ^{15}N) have a low gyromagnetic ratio which makes it difficult to provide images with very high spatial resolution because the gradient strengths of conventional MRI systems is limited and usually optimised for protons. Furthermore, in ^{13}C MRI co-registration with a high-resolution proton image is necessary to obtain anatomical information. However, optimal co-registration of ^{1}H and ^{13}C MRI images requires the application of double resonant coils, which is technically demanding and thus expensive. Our imaging approach can be used for virtually every molecule that can be polarised via PHIP, which comprises a large amount of biological relevant molecules, for example, succinate (component of the citrate cycle) [105] or barbiturates [106]. This variability in combination with the simplicity of our method may result in widespread usage in MRI.

4. STORAGE OF HYPERPOLARISATION IN SINGLET STATES

4.1. Theory

A drawback of hyperpolarisation in solution NMR experiments is the limited lifetime of the nuclear spin order which relaxes to the thermal equilibrium with the T_1 (spin-lattice) relaxation time, typically on the order of seconds in ^{1}H NMR. A possible solution for this issue relies on the creation of long-lived singlet states to prolong the lifetime of the hyperpolarisation [21,68,69]. Indeed, it was shown that the lifetimes of spin-singlet states can be longer than the spin-lattice relaxation times of the constituent spins up to a factor of 37 [107]. These long-lasting states require a pair of isolated (strongly coupled) spins $I = 1/2$. Because of the spin-singlet states' symmetry, those relaxation mechanisms which are symmetric to spin exchange are

inactive. One of these is the dipole–dipole relaxation mechanism which is dominant in liquid-state NMR.

In the pioneering paper, Carravetta, Johannessen and Levitt [21] demonstrated the possibility to deposit singlet-state order even though the singlet state is not an eigenstate of the spin system. The trick is to switch the symmetry of the spin interactions at different points during the experimental procedure. When exchange symmetry is imposed, coherent singlet–triplet transitions are suppressed and the lifetime of the singlet state is extended.

In a typical NMR experiment, the initial state is given by the Boltzmann distribution which results in a small population difference of the eigenstates (typically on the order 10^{-4} to 10^{-5}) in presence of a magnetic field B_0. Assuming the system is a nonequivalent weakly coupled spin pair, the singlet-state NMR experiment consists of three steps:

1. *Singlet-state creation*: Transform nuclear spin magnetisation (which is a property of the triplet manifold) into nuclear singlet order. This step can be done in several different ways, the most commonly used is the application of a dedicated pulse sequence known as M2S [22,23]. It consists of two trains of π pulses, the temporal window between the pulses is carefully synchronised with the evolutions due to scalar coupling and chemical shifts of the particular pair.
2. *Singlet preservation*: Once the singlet state is created, spin-exchange symmetry is imposed to eliminate singlet–triplet transitions. For a weakly coupled system, the strategy consists in keeping the system as if it was a strongly coupled one. To achieve this, different methods can be used: field cycling (moving the sample to a negligible magnetic field B_0), pulse sequences or applications of long rf pulses, which, even under a strong B_0, are able to create an *effective* small magnetic field.
3. *Conversion to observable magnetisation*: Because nuclear singlet order is nonmagnetic, observation of the singlet-derived NMR signals requires the reconversion into nuclear spin magnetisation. This can be done simply by stopping the step 2 and, in this way, restoring the coherent singlet–triplet transitions.

It is particularly beneficial to generate such singlet states involving two protons, as their signal is the highest among the nuclei usually applied in NMR and their relaxation times are rather short at ambient conditions. The strong coupling of the nuclei can be easily fulfilled at low magnetic fields where chemical shift differences are naturally vanishing [21,24,69,108]. In high magnetic fields, which have the advantage of high spectral resolution and thus site selectivity, this magnetic equivalence is more difficult to achieve

and requires the use of dedicated pulse sequences to minimise the evolution of the spin system due to the chemical shift [68,109].

As the pH_2 molecule itself forms a singlet state, the hydrogenation reaction in PHIP not only produces enhanced polarisation but can also generate long-lived proton singlet states making it an excellent candidate for many applications in natural sciences [4,110,111]. Indeed, such long-lived PHIP states have been exploited in low or even zero magnetic fields [24,25,70].

In previous works [26,27], we have shown that when acetylenedicarboxylic acid dimethyl ester is hydrogenated with parahydrogen to generate maleic acid dimethyl ester, the pH_2 occupies chemically equivalent vinylene (V) positions in the symmetric molecule. Consequently, both spins remain strongly J-coupled for every magnetic field. With this, the first two steps of the singlet-state experiments are avoided:

1. *Singlet-state creation*: The singlet state comes naturally from the initial pH_2 singlet state.
2. *Singlet-state preservation*: The singlet state remains an eigenstate, because the system is strongly coupled for every magnetic field. It was shown that the hyperpolarised signal can be stored in a symmetric molecule as a singlet state, prolonging its lifetime from $T_1 = 15$ s to $T_{\text{Singlet}} = 4$ min.
3. *Conversion to observable magnetisation*: This is more difficult to accomplish. The main findings achieved on this will be recapitulated in the following.

Preserving the long-lived singlet state inside the magnet is needed for applications of hyperpolarisation, for example, in biomedical analysis. By DNP and rf pulse sequences, Warren *et al.* [19] were able to create singlet-state population at high field, and observed it by subsequently breaking the singlet symmetry by chemical means, thus changing the spin system. Another important contribution, which also used DNP to create an initially enhanced magnetisation, was presented by Vasos *et al.* [112]. There, the initial hyperpolarised ^{13}C magnetisation was transferred to ^{1}H, converted into a long-lived state and then read out by partially reconverting it into observable proton magnetisation. This extended the lifetime of the ^{1}H polarisation by a factor of 7 to $T_{\text{Singlet}} = 16$ s. Feng *et al.* [113] recently showed that storage of the proton polarisation in a ^{13}C singlet state causes a 69-fold extension of the life time. An important step towards biomedical applications is the work reported by Pileio *et al.* [114], where the enhanced nuclear polarisation obtained by DNP is observed, even used for MRI experiments, and subsequently returned into singlet order.

4.2. Conversion Methods

4.2.1 Field Cycling

When acetylenedicarboxylic acid dimethyl ester is hydrogenated with parahydrogen (Fig. 4.18A), the pH_2 occupy chemically equivalent vinylene (V) positions in the symmetric molecule. Consequently, the spins remain strongly J-coupled for every magnetic field. At high field, the molecule represents an $AA'XX'$ spin system (Fig. 4.18B). The vinylene protons, V and V', the former pH_2 protons, exhibit a coupling $J_{VV'} = 11.6$ Hz, while the long-range couplings to the methyl protons (M) are expected to be lower by an order of magnitude.

The energy levels associated with the singlet and triplet states of the pH_2 in the vinylene group, $S_0^{VV'}$ and $T_{+1}^{VV'}$ as a function of the preparation field B_0 can easily be calculated from the Hamiltonian of the spin system,

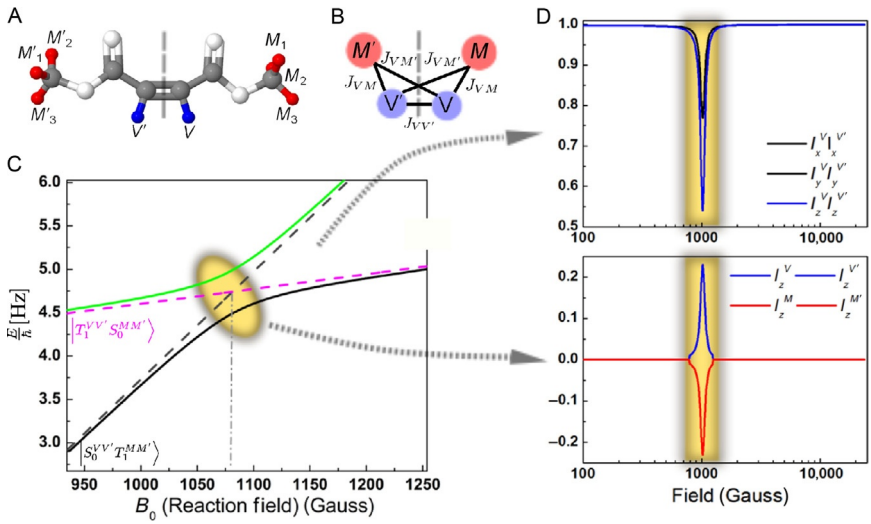

Figure 4.18 Symmetrical molecule, energy levels and density matrix operators. (A) Maleic acid dimethyl ester with labelled protons. (B) Sketch of the J-coupling network between the vinylene (V and V') and methyl protons (M_{1-3} and M'_{1-3}), $J_{VV'} = 11.6$ Hz; long-range couplings have been assumed to the methyl ($J_{VM} = 0.75$ Hz and $J_{VM'} = 0.25$ Hz). (C) Two of the 16 energy levels for the four-spin system. Note the level anti-crossing at 0.11 T between the singlet and the triplet state of the pair VV′, defining the resonance condition. The dashed lines correspond to the exact eigenvalues when a magnetically equivalent molecule is assumed ($J_{VM} = J_{VM'}$). (D) Upper panel: expectation values of the singlet-state operators. Bottom panel: expectation values of the observable polarisation operators. Remarkably, the calculated expectation values remain unchanged for every field except for the resonance field (0.11 T).

$$H = \nu_V\left(I_z^V + I_z^{V'}\right) + \nu_M\left(I_z^M + I_z^{M'}\right) + J_{VV'}I^V \cdot I^{V'} + J_{VM}\left(I^V \cdot I^M + I^{V'} \cdot I^{M'}\right) + J_{VM'}\left(I^V \cdot I^{M'} + I^{V'} \cdot I^M\right) \tag{4.4}$$

two of the levels are plotted in Fig. 4.18C. The dashed lines correspond to the eigenvalues $\left|S_0^{VV'}T_{+1}^{MM'}\right\rangle$ and $\left|T_{+1}^{VV'}S_0^{MM'}\right\rangle$ obtained when the two vinylene protons are treated as magnetically equivalent, that is, $J_{VM}=J_{VM'}$. They cross at a well-defined field $B_0=1080$ Gauss (resonance condition). The magnetic field for the resonance condition, B_R, can be calculated from the following expression:

$$(\nu_V - \nu_M)|_{B_R} = J_{VV'} \tag{4.5}$$

that is, the magnetic field B_R is such that the chemical shift among the vinylene and the methyl groups matches the coupling among the pH_2 pair.

Energy level crossings, in which two quantum states cross as a function of an external parameter, are ubiquitous in quantum mechanics [115]. Small off-diagonal elements in the Hamiltonian, however, lead to level anti-crossing (or avoided crossing) and the eigenstates are mixed [19,27,115–118]. In our case, such off-diagonal terms mixing singlet and triplet states occur if $J_{VM}\neq J_{VM'}$. This condition does not interfere with the symmetry of the molecule (for details see Ref. [27]). The slightly changed energy values are shown as solid lines in Fig. 4.18C. The external control parameter (B_0) can be varied in time such that the system traverses the anti-crossing region. Then, a transition from one branch to the other, in our case singlet to triplet or vice versa, is possible with a probability that depends on the external parameter sweep rate. This idea was first described theoretically by Landau and Zener [116,117] and studied experimentally and theoretically in a number of different physical systems including PHIP and NMR [19,67,119].

From Fig. 4.18C, we infer that for preparation fields different from the resonance field for anti-crossing the singlet state is disconnected from the triplet state. Consequently, an initial singlet state that arises from a PHIP reaction inside the magnet will remain a singlet state and will not be affected by conventional spin-lattice relaxation mechanisms. Sweeping the field (or the sample) through the level anti-crossing region, on the other hand, offers a simple way of generating a polarised triplet state in a controlled way.

The singlet–triplet conversion can quantitatively be calculated for different preparation fields B_0 for the hydrogenation reaction according to the Liouville–von Neumann equation with the Hamiltonian of Eq. (4.4) [27]. The initial

state that corresponds to the singlet pH_2 VV' protons can be written in terms of density operators as $\rho(0) = \frac{1}{4}I - \left(I_x^V I_x^{V'} + I_y^V I_y^{V'} + I_z^V I_z^{V'}\right)$ [118,119], neglecting the contributions arising in the thermal equilibrium magnetisation.

In Fig. 4.18D, the expectation values of the spin operators are plotted for magnetic fields close to the resonance field. Remarkably, the expectation values related to the singlet state remain unchanged for all fields except for the resonance field associated with the anti-crossing, when part of the singlet state is converted into observable polarisation. As can be seen in the bottom panel of Fig. 4.18D, the total angular momentum remains zero and is conserved in the four-particle system comprised of the pairs of the vinyl and the methyl protons VV' and MM'. The controlled singlet–triplet conversion via level anti-crossing thus offers a simple way of generating highly polarised species in high magnetic fields, limited by relaxation of the singlet rather than the triplet state. It should also be noted that only a fraction of the singlet state is converted to a triplet at the resonance field in a single sweep while another fraction remains stored, it will be shown that it is possible to take advantage of this fact by generating multiconversions.

These theoretical considerations were validated experimentally. When a 90° pulse is applied following a short waiting time (T_W) after the start of the chemical reaction, the acquired NMR spectrum shows the thermally polarised methyl protons only (Fig. 4.19, left). This is due to the fact that the created singlet state itself is silent in magnetic resonance. If the sample is quickly moved to the resonance field and back to the high detection field on a timescale much shorter than $T_1 \approx 15$ s, singlet–triplet conversion occurs and a hyperpolarised antiphase spectrum of vinylene and methyl protons is observed (Fig. 4.19, right). This demonstrates the controlled singlet–triplet conversion.

The lifetime of the single state ($T_{Singlet}$) in the high magnetic field (7 T) can be measured using the same protocol with variable waiting times T_W. For every T_W a spectrum was recorded in which the intensity of the peak corresponding to the vinylene group was determined. These data plotted as a function of T_W were fitted to an exponential decay yielding a lifetime $T_{Singlet}$ as long as 4 min [26].

4.2.2 Radiofrequency Pulse Sequences

Alternatively to the field-cycling method, the singlet nuclear spin state can be converted into measurable magnetisation by using an rf pulse sequence at the observation field. This reduces the technical effort, since an accurate, reproducible field cycling would require a complex sample cycling system.

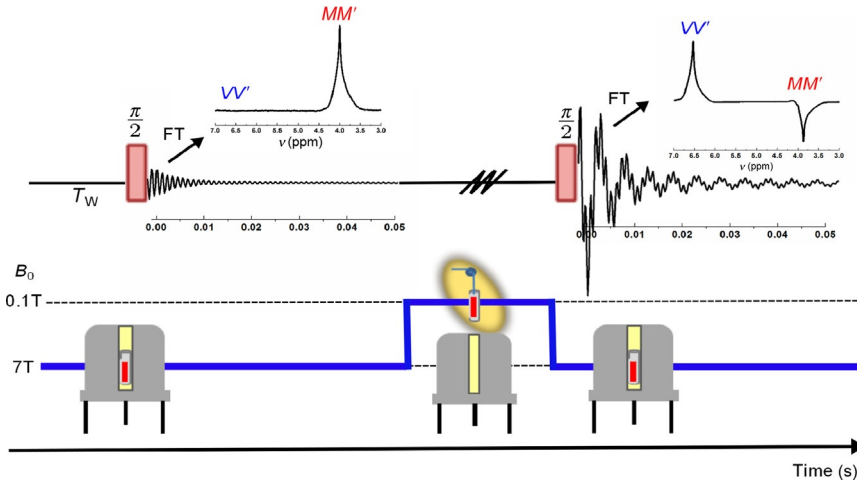

Figure 4.19 Preservation and observation of the pH_2 singlet state at 7 Tesla. Top: scheme of the pulse sequence, the observed FID signals and respective spectra at 7 T before and after the mixing between the singlet and triplet states is allowed (at 0.11 T). Bottom: the magnetic field path followed by the sample (bold line).

Moreover, for *in vivo* applications, the field-cycling method is not applicable since, for example, it is not practicable to transport an animal or a human being to a certain magnetic field during an MRI acquisition.

It is possible to perform the singlet–triplet conversion by using rf pulses to scale the chemical shift part of the relevant Hamiltonian and thereby to access the level anti-crossing region. The use of rf pulses to scale the Hamiltonian inside the magnet is a common strategy in traditional NMR.

Many sequences exist which can perform this task. So far, the singlet–triplet conversion of the ^{1}H singlet state in dimethyl maleate was achieved by a long constant rf pulse [28]. When applying a long rf pulse the chemical shift of the Hamiltonian is rescaled. To understand this effect, we first re-evaluate the unperturbed Hamiltonian in Eq. (4.4) which in the rotating frame is given by:

$$\breve{H} = \Omega_V \left(I_z^V + I_z^{V'} \right) + \Omega_M \left(I_z^M + I_z^{M'} \right) + J\text{-terms} \tag{4.6}$$

where $\Omega_K = 2\pi(\nu_K - \nu_{\text{ref}})$ (with $K \in \{V,M\}$) with ν_{ref} being the rotation frequency of the rotating frame. The J-coupling terms are invariant operators under the rf modulation and therefore will be excluded in the following calculations.

The Hamiltonian can be rewritten by using $I_j^{KK'} = I_j^K + I_j^{K'}$ ($\forall j \in \{x,y,z\}$, $K \in \{V,M\}$) and introducing $\Delta\omega = \frac{1}{2}(\Omega_V + \Omega_M)$ and $\Delta\Omega = \frac{1}{2}(\Omega_V - \Omega_M)$:

$$H = \Delta\omega\left(I_z^{VV'} + I_z^{MM'}\right) + \Delta\Omega\left(I_z^{VV'} - I_z^{MM'}\right), \tag{4.7}$$

wherein the singlet–triplet conversion is caused by the second antisymmetric term. Under rf perturbation, the Hamiltonian takes the form:

$$H = \omega_1\left(I_x^V + I_x^{V'} + I_x^M + I_x^{M'}\right) + \Omega_V\left(I_z^V + I_z^{V'}\right) + \Omega_M\left(I_z^M + I_z^{M'}\right), \tag{4.8}$$

in which ω_1 is the rf strength of the pulse and the reference frequency was set to the carrier rf frequency: $\omega_{\text{ref}} = \omega_{\text{rf}}$. This Hamiltonian can again be rewritten as:

$$H = \omega_1\left(I_x^{VV'} + I_x^{MM'}\right) + \Delta\omega\left(I_z^{VV'} + I_z^{MM'}\right) + \Delta\Omega\left(I_z^{VV'} - I_z^{MM'}\right). \tag{4.9}$$

To clarify the effect of this Hamiltonian, it is transformed into another rotating frame, rotating around the effective rotation axis $\vec{\omega}_{\text{eff}} = \omega_{\text{eff}}\left(\sin(\theta)\vec{e}_x + \cos(\theta)\vec{e}_z\right)$ with $\omega_{\text{eff}} = \sqrt{\omega_1^2 + \Delta\omega^2}$ and $\tan(\theta) = \dfrac{\omega_1}{\Delta\omega}$:

$$\begin{aligned}\widetilde{H} = {} & \omega_{\text{eff}}\left(I_{z'}^{VV'} + I_{z'}^{MM'}\right) + \cos(\theta)\Delta\omega\left(I_{z'}^{VV'} - I_{z'}^{MM'}\right) \\ & - \sin(\theta)\Delta\Omega\left(I_{x'}^{VV'} - I_{x'}^{MM'}\right).\end{aligned} \tag{4.10}$$

The third term on the right side has only nonsecular contributions and can therefore be neglected in the secular approximation. The second antisymmetric term which causes the singlet–triplet conversion can be adjusted by an adequate choice of the rf pulse strength and the carrier frequency to satisfy the new resonance condition:

$$\cos(\theta)(\nu_V - \nu_M)|_{B_0} = J_{VV'}, \tag{4.11}$$

where B_0 is the observation field. Hence, after the parameters are properly chosen for the anti-crossing to be reached, the population is partially transferred from the singlet state to measurable magnetisation (as mentioned before the amount of conversion depends on how the anti-crossing is traversed). As in the field-cycling method (Fig. 4.19), the vinylene group peak and the methyl group peak show a phase difference of 180° (Fig. 4.20).

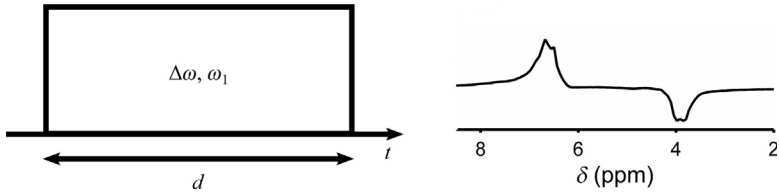

Figure 4.20 Left: Long constant rf pulse able to realise the transition of the singlet spin state into measurable magnetisation. Right: example spectrum acquired using the long rf pulse with a duration d of 5 s, an rf pulse strength of $\omega_1 = 1360$ Hz and a carrier frequency offset of $\Delta\omega = 100$ Hz.

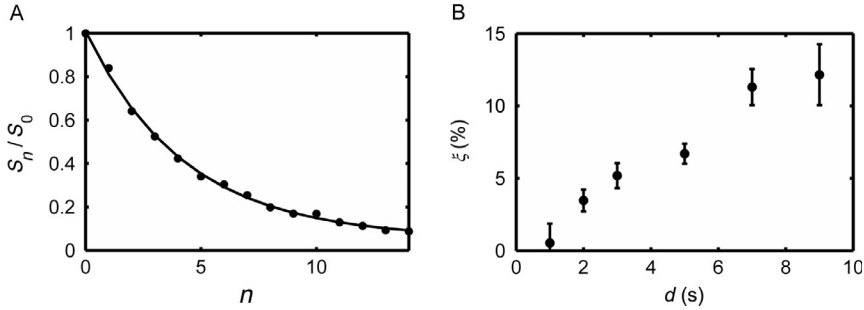

Figure 4.21 (A) Exponential decay of the vinylene group signal of dimethyl maleate in a series of multiple conversions of the singlet state to measurable magnetisation. The signal was normalised by the signal S_0 acquired after the first conversion. The solid line shows the exponential fit to the data with a characteristic decay constant of D_c. (B) Conversion fraction ξ of the constant long pulse as a function of the pulse duration.

The use of rf pulse sequences has the additional advantage that it enables performing series of multiple conversions in a controlled way. This allows to use the generated hyperpolarisation more efficiently, especially if the converted fraction per conversion is low. As it can be seen in Fig. 4.21A, the signal decays exponentially as a function of the number of applied conversions, n.

A detailed analysis of this behaviour [28] showed that the characteristic constant D_c of the exponential decay is a function of the converted fraction per conversion ξ as well as of the lifetime of singlet spin state T_{Singlet}:

$$\frac{S_n}{S_0} = \mathrm{e}^{-D_c n} \tag{4.12}$$

$$D_c = \frac{1}{T_{\text{Singlet}}}\text{TR} - \ln(1-\xi) \tag{4.13}$$

Performing this experiment for different repetition times allows the determination of both parameters, T_{Singlet} and ξ. In Fig. 4.21B, the dependency of the converted fraction as a function of the duration d of the long constant pulse is shown.

The conversion fraction is increasing monotonically with the duration of the pulse since there is more time for the spin system to convert singlet spin order to measurable magnetisation. However, this does not necessarily imply larger measurable magnetisation for longer rf pulses since the converted magnetisation is relaxing with the fast longitudinal relaxation time T_1. In a simplified classical model, a constant conversion rate k between the singlet and the triplet state can be assumed whereat the triplet state relaxes with T_1 to the thermal polarisation and the singlet state relaxes with T_{Singlet} (Fig. 4.22A).

In the following analysis, the thermal polarisation as well as the relaxation of the singlet state is neglected. This leads to the following differential

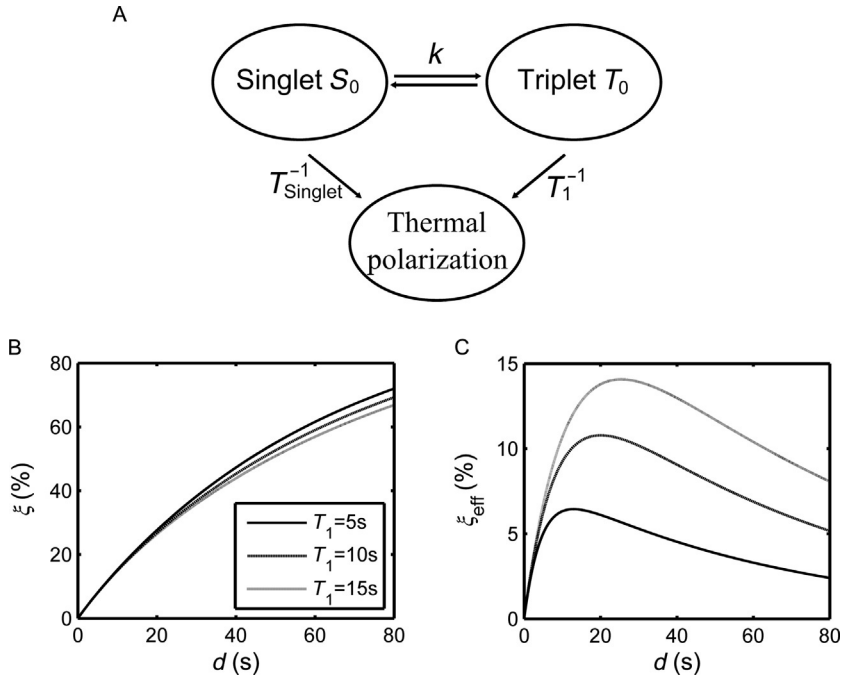

Figure 4.22 (A) Model of the singlet–triplet conversion during the rf perturbation. A constant conversion rate k is assumed during the pulse. (B) Conversion fraction ξ and effective conversion fraction ξ_{eff} calculated with Eqs. (4.16) and (4.17) using $k = 0.017\,\text{s}^{-1}$ and $T_1 = 5$, 10 and 15 s.

equations which describe the population of singlet state A_{Singlet} and the population of triplet state A_{Triplet}:

$$\begin{aligned}\frac{\mathrm{d}A_{\text{Singlet}}}{\mathrm{d}t} &= -k\left(A_{\text{Singlet}} - A_{\text{Triplet}}\right)\\ \frac{\mathrm{d}A_{\text{Triplet}}}{\mathrm{d}t} &= -k\left(A_{\text{Triplet}} - A_{\text{Singlet}}\right) - \frac{1}{T_1}A_{\text{Triplet}}.\end{aligned} \tag{4.14}$$

With the boundary conditions $A_{\text{Singlet}}(t=0) = A^0_{\text{Singlet}}$, $A_{\text{Triplet}}(t=0) = 0$ and $A_{\text{Triplet}}(t\to\infty) = 0$, the solution of these differential equations is given by:

$$\begin{aligned}A_{\text{Singlet}} &= \frac{A^0_{\text{Singlet}}}{k_2 - k_1}\left[\left(k + \frac{1}{T_1} - k_1\right)\exp(-k_1 t) - \left(k + \frac{1}{T_1} - k_2\right)\exp(-k_2 t)\right]\\ A_{\text{Triplet}} &= \frac{A^0_{\text{Singlet}}k}{k_2 - k_1}\left[\exp(-k_1 t) - \exp(-k_2 t)\right]\end{aligned} \tag{4.15}$$

with the characteristic exponential decay rates $k_{1,2} = k + \frac{1}{2T_1} \pm \sqrt{k^2 + \left(\frac{1}{2T_1}\right)^2}$. The conversion fraction ξ after a pulse with duration d, that is, the relative loss of singlet-state population, is given by:

$$\xi(d) = \frac{A^0_{\text{Singlet}} - A_{\text{Singlet}}(t=d)}{A^0_{\text{Singlet}}}. \tag{4.16}$$

In contrast, the fraction of the singlet state that is converted into measurable magnetisation, which will be called effective conversion in the following, is given by:

$$\xi_{\text{eff}}(d) = \frac{A_{\text{Triplet}}(t=d)}{A^0_{\text{Singlet}}}. \tag{4.17}$$

The conversion rate k is given by the slope of the conversion reaction ξ at $d=0$: $\frac{\partial\xi}{\partial d}|_{d=0} = k$. For the long constant pulse with an rf strength ω_1 of 1360 Hz and the associated offset $\Delta\omega$ of 100 Hz, the initial slope leads to a conversion rate of $k = 0.017\,\text{s}^{-1}$. For this conversion rate, the dependence of the conversion fraction ξ and the effective conversion fraction ξ_{eff} on the long rf pulse length d, according to Eqs. (4.16) and (4.17), is shown for three different values of T_1 in Fig. 4.22B and C, respectively.

In general, the optimal duration d and the maximum achievable effective conversion ξ_{eff} decrease for shorter T_1 (Fig. 4.22C). However, for example,

for dimethyl maleate a maximum of the measurable magnetisation was found experimentally for an rf pulse duration of $d \approx 5\,\mathrm{s}$ ($\omega_1 = 1360\,\mathrm{Hz}$ and $\Delta\omega = 100\,\mathrm{Hz}$). According to Eq. (4.17), this would correspond to a T_1 relaxation time of around 1.4 s, which is shorter than the real T_1 relaxation time of 10 s for the vinylene protons in the molecule. This deviation is caused by the saturation effect of the rf pulse.

4.2.3 Conclusion

In this chapter, we showed the possibility to store ^{1}H PHIP in the singlet spin state of a symmetric molecule for minutes at high magnetic fields. The stored hyperpolarisation can be converted into measurable magnetisation either by field cycling or by rf pulse sequences which both are physically based on a level anti-crossing phenomenon. This long lifetime of the hyperpolarisation opens up new applications of hyperpolarisation in spectroscopy and imaging which is of particular importance for ^{1}H NMR due to the relatively short T_1 relaxation times in comparison to non-proton nuclei like ^{13}C. Particularly with regard to future biological and medical applications, the storage of ^{1}H hyperpolarisation in long-lived ^{1}H spin states enables to perform *in vivo* hyperpolarisation experiments on the standard nuclear spin of clinical MR tomographs without the necessity of additional MR hardware like broadband amplifiers and adapted coils. For this purpose, the hyperpolarisation method PHIP has the advantage that the singlet nuclear ^{1}H spin state is intrinsically generated.

5. CONCLUSION

In this contribution, we have demonstrated that the hyperpolarisation of proton nuclear spins is a valuable method to increase the sensitivity of ^{1}H NMR spectroscopy and ^{1}H MRI despite the short lifetime of proton hyperpolarisation. We addressed this important lifetime issue with two different concepts, namely, the production of hyperpolarised liquids in a continuous flow fashion and the storage of hyperpolarisation in slowly relaxing singlet states. The continuous flow approach was demonstrated with Overhauser DNP, being the only DNP method where hyperpolarisation takes place in the liquid phase. Overhauser DNP provides only moderate enhancements compared to solid-state DNP and, even more notably, compared to dissolution DNP but its fast polarisation build-up and applicability in liquids renders it the DNP method of choice for the continuous production of hyperpolarised liquids. Also PHIP qualifies for the continuous generation

of hyperpolarised molecules, as we have shown in a previous publication [120]. Here, the continuous application of parahydrogen by the use of hollow fibre membranes is the key feature. In contrast to continuous DNP experiments, for which the duration is virtually unlimited, in hydrogenative PHIP experiments the amount of unsaturated precursor is the limiting factor for the available time of continuous signal enhancement. However, the extension of this concept to the SABRE method would result in continuous hyperpolarisation that can last many hours as no precursor is consumed.

The second approach for the extension of the hyperpolarisation lifetime; that is, the usage of singlet states, was accomplished in our contribution for PHIP experiments, which is especially intriguing as parahydrogen possesses singlet symmetry already. We have demonstrated that the parahydrogen singlet state can be preserved at nearly every magnetic field strength, if parahydrogen is embedded in a symmetrical molecule. This approach resulted in the surprisingly long lifetime of the hyperpolarised proton singlet state of 4 min. In these experiments, the conversion of the NMR-silent singlet state to an observable triplet state is a difficult task and was achieved by exploiting the existence of level anti-crossings. We showed that the singlet states can be assessed either by a field-cycling method or by using a dedicated pulse sequence. Of course, the usage of singlet states for prolongation of the hyperpolarisation lifetime is a general concept and was used also for molecules polarised via DNP. In this case, an additional experimental step has to be performed, that is, the conversion of the initial hyperpolarisation into a singlet state.

The second issue that arises in hyperpolarised proton NMR and MRI is the generation of contrast between a small amount of hyperpolarised molecules and a vast thermal background signal. This problem is especially severe if *in vivo* applications are sought because of the large amount of protons being present in the body. In this contribution, we have shown that we can use the special signal pattern that comes along with the hyperpolarisation method (180° phase shift for Overhauser DNP and longitudinal two-spin order giving rise to antiphase signals for PHIP). In our DNP experiments, we have demonstrated that we can unambiguously distinguish hyperpolarised from thermally polarised water even for small signal enhancements if we calculate the phase map of the corresponding MR images. For PHIP ^{1}H MRI, we make use of the J-coupling-induced refocusing of the antiphase signal that occurs for specific echo times. This imaging method in combination with the very large signal enhancement associated with PHIP gives rise to an outstanding contrast in ^{1}H MRI.

If we are able to use the standard NMR and MRI nucleus ^{1}H for MRI of hyperpolarised substances, we can greatly facilitate the technical demands and costs that come along with MRI of hetero-nuclei like ^{13}C and ^{15}N. MRI of hetero-nuclei requires costly isotope labelling of the applied substances, adaption of pulse sequences and special equipment like double resonant coils and broadband amplifiers. In contrast, hyperpolarised ^{1}H MRI can be performed with conventional pulse sequences and hardware and without the necessity of using isotope-enriched substances. Additionally, at a given maximum gradient strength, ^{1}H MRI provides a higher spatial resolution as ^{13}C or ^{15}N MRI because of the higher gyromagnetic ratio of ^{1}H.

Another general problem of PHIP and DNP is that stable and mostly toxic polarising agents have to be added to the sample, which is especially problematic for biomedical applications. These comprise free radicals in the case of DNP and transition metal catalysts for PHIP. Here, we described two methods that facilitate a simple and reliable separation of radicals and hyperpolarised molecules for DNP. Both methods rely on the covalent bonding of the radical to a polymer matrix which is a thermoresponsive hydrogel in the first case and sepharose beads in the second case. We demonstrated that both methods produce radical-free hyperpolarised liquids with unaltered T_1 relaxation times which is especially important for our implementation of continuous flow DNP. Currently, we are trying to extend this concept for the immobilisation of PHIP catalysts. Here, the sterical hindrance that arises from covalent bonding of the catalyst to a polymer matrix might be a problem and results in a reduced PHIP efficiency. However, we have shown in a former work that we are able to hyperpolarise a biocompatible hyperbranched polymer which exhibited terminal alkyne groups with a standard PHIP catalyst [121]. We reached a signal enhancement for protons of more than 1000-fold in this also sterical hindered case and thus do hope that we will be able to efficiently hyperpolarise a small molecule with a covalently bound catalyst.

Both of the used hyperpolarisation methods have certain merits and disadvantages and the choice of the method depends always on the specific scientific question or application. DNP and PHIP are able to polarise molecules in the gas (PHIP), liquid (PHIP, DNP) and solid (DNP) phase. DNP has the great advantage that it can virtually polarise every molecule, whereas the application of PHIP is restricted to unsaturated compounds or molecules that can bind to a transition metal catalyst (SABRE). However, PHIP reaches higher polarisation levels than Overhauser DNP and is less technically demanding, but it requires chemical expertise. Finally, we have

demonstrated in this contribution that both methods are well suited for the generation of ^{1}H hyperpolarised molecules.

ACKNOWLEDGEMENTS

The authors gratefully acknowledge financial support from the Max Planck Society, the Max Planck Graduate Center with the Johannes Gutenberg-University Mainz (MPGC), the Federal Ministry of Education and Research within the program "Validierung des Innovationspotenzials wissenschaftlicher Forschung—VIP" (VIP0327) and the COST action TD 1103.

REFERENCES

[1] A.W. Overhauser, Polarization of nuclei in metals, Phys. Rev. 92 (1953) 411.
[2] A. Abragam, M. Goldman, Principles of dynamic nuclear-polarization, Rep. Prog. Phys. 41 (1978) 395.
[3] C.R. Bowers, D.P. Weitekamp, Transformation of symmetrization order to nuclear-spin magnetization by chemical-reaction and nuclear-magnetic-resonance, Phys. Rev. Lett. 57 (1986) 2645.
[4] K. Münnemann, H.W. Spiess, Nuclear magnetic resonance the art of signal enhancement, Nat. Phys. 7 (2011) 522.
[5] R.A. Green, R.W. Adams, S.B. Duckett, R.E. Mewis, D.C. Williamson, G.G.R. Green, The theory and practice of hyperpolarization in magnetic resonance using parahydrogen, Prog. Nucl. Magn. Reson. Spectrosc. 67 (2012) 1.
[6] N.D. Bhaskar, W. Happer, T. Mcclelland, Efficiency of spin exchange between rubidium spins and Xe-129 nuclei in a gas, Phys. Rev. Lett. 49 (1982) 25.
[7] T.G. Walker, W. Happer, Spin-exchange optical pumping of noble-gas nuclei, Rev. Mod. Phys. 69 (1997) 629.
[8] R.H. Acosta, P. Blümler, K. Münnemann, H.W. Spiess, Mixture and dissolution of laser polarized noble gases: spectroscopic and imaging applications, Prog. Nucl. Magn. Reson. Spectrosc. 66 (2012) 40.
[9] J.H. Ardenkjær-Larsen, B. Fridlund, A. Gram, G. Hansson, L. Hansson, M.H. Lerche, et al., Increase in signal-to-noise ratio of > 10,000 times in liquid-state NMR, Proc. Natl. Acad. Sci. USA 100 (2003) 10158.
[10] K. Golman, R.I. Zandt, M. Lerche, R. Pehrson, J.H. Ardenkjær-Larsen, Metabolic imaging by hyperpolarized C-13 magnetic resonance imaging for in vivo tumor diagnosis, Cancer Res. 66 (2006) 10855.
[11] D.M. Wilson, K.R. Keshari, P.E.Z. Larson, A.P. Chen, S. Hu, M. Van Criekinge, et al., Multi-compound polarization by DNP allows simultaneous assessment of multiple enzymatic activities in vivo, J. Magn. Reson. 205 (2010) 141.
[12] N.M. Zacharias, H.R. Chan, N. Sailasuta, B.D. Ross, P. Bhattacharya, Real-time molecular imaging of tricarboxylic acid cycle metabolism in vivo by hyperpolarized 1-C-13 diethyl succinate, J. Am. Chem. Soc. 134 (2012) 934.
[13] F.A. Gallagher, M.I. Kettunen, S.E. Day, D.E. Hu, J.H. Ardenkjær-Larsen, R.I. Zandt, et al., Magnetic resonance imaging of pH in vivo using hyperpolarized (13)C-labelled bicarbonate, Nature 453 (2008) 940.
[14] Y. Lee, G.S. Heo, H.F. Zeng, K.L. Wooley, C. Hilty, Detection of living anionic species in polymerization reactions using hyperpolarized NMR, J. Am. Chem. Soc. 135 (2013) 4636.

[15] L.S. Bouchard, S.R. Burt, M.S. Anwar, K.V. Kovtunov, I.V. Koptyug, A. Pines, NMR imaging of catalytic hydrogenation in microreactors with the use of para-hydrogen, Science 319 (2008) 442.
[16] M. Duewel, N. Vogel, C.K. Weiss, K. Landfester, H.W. Spiess, K. Münnemann, Online monitoring of styrene polymerization in mini emulsion by hyperpolarized (129)xenon NMR spectroscopy, Macromolecules 45 (2012) 1839.
[17] S. Ebert, A. Amar, C. Bauer, M. Kölzer, P. Blümler, H. Spiess, et al., A mobile DNP polarizer for continuous flow applications, Appl. Magn. Reson. 43 (2012) 195.
[18] J.F. Dechent, L. Buljubasich, L.M. Schreiber, H.W. Spiess, K. Münnemann, Proton magnetic resonance imaging with para-hydrogen induced polarization, Phys. Chem. Chem. Phys. 14 (2012) 2346.
[19] W.S. Warren, E. Jenista, R.T. Branca, X. Chen, Increasing hyperpolarized spin lifetimes through true singlet Eigenstates, Science 323 (2009) 1711.
[20] M.H. Levitt, Singlet nuclear magnetic resonance, Annu. Rev. Phys. Chem. 63 (2012) 89.
[21] M. Carravetta, O.G. Johannessen, M.H. Levitt, Beyond the T-1 limit: singlet nuclear spin states in low magnetic fields, Phys. Rev. Lett. 92 (2004) 153003.
[22] G. Pileio, M. Carravetta, M.H. Levitt, Storage of nuclear magnetization as long-lived singlet order in low magnetic field, Proc. Natl. Acad. Sci. USA 107 (2010) 17135.
[23] M.C.D. Tayler, M.H. Levitt, Singlet nuclear magnetic resonance of nearly-equivalent spins, Phys. Chem. Chem. Phys. 13 (2011) 5556.
[24] D. Canet, S. Bouguet-Bonnet, C. Aroulanda, F. Reineri, About long-lived nuclear spin states involved in para-hydrogenated molecules, J. Am. Chem. Soc. 129 (2007) 1445.
[25] E. Vinogradov, A.K. Grant, Hyperpolarized long-lived states in solution NMR: three-spin case study in low field, J. Magn. Reson. 194 (2008) 46.
[26] M.B. Franzoni, L. Buljubasich, H.W. Spiess, K. Münnemann, Long-lived H-1 singlet spin states originating from para-hydrogen in Cs-symmetric molecules stored for minutes in high magnetic fields, J. Am. Chem. Soc. 134 (2012) 10393.
[27] L. Buljubasich, M.B. Franzoni, H.W. Spiess, K. Münnemann, Level anti-crossings in parahydrogen induced polarization experiments with Cs-symmetric molecules, J. Magn. Reson. 219 (2012) 33.
[28] M.B. Franzoni, D. Graafen, L. Buljubasich, L.M. Schreiber, H.W. Spiess, K. Münnemann, Hyperpolarized H-1 long lived states originating from parahydrogen accessed by rf irradiation, Phys. Chem. Chem. Phys. 15 (2013) 17233.
[29] K.H. Hausser, D. Stehlik, Dynamic nuclear polarization in liquids, Adv. Magn. Reson. 3 (1968) 79.
[30] J. Potenza, Measurement and applications of dynamic nuclear polarization, Adv. Mol. Relax. Int. Proc. 4 (1972) 229.
[31] W. Müller-Warmuth, K. Meise-Gresch, Molecular motions and interactions as studied by dynamic nuclear-polarization (dnp) in free-radical solutions, Adv. Magn. Reson. 11 (1983) 1.
[32] R.A. Dwek, R.E. Richards, D. Taylor, Nuclear electron double resonance in liquids, in: E.F. Mooney (Ed.), Annual Reports on NMR Spectroscopy, vol. 2, Academic Press, London, 1969, pp. 293–344.
[33] M.D. Lingwood, S. Han, Solution-state dynamic nuclear polarization, in: G.A. Webb (Ed.), Annual Reports on NMR Spectroscopy, vol. 73, Academic Press, London, 2011, pp. 83–126.
[34] C. Griesinger, M. Bennati, H.M. Vieth, C. Luchinat, G. Parigi, P. Höfer, et al., Dynamic nuclear polarization at high magnetic fields in liquids, Prog. Nucl. Magn. Reson. Spectrosc. 64 (2012) 4.

[35] S. Garcia, J.H. Walton, B. Armstrong, S. Han, M.J. McCarthy, L-band Overhauser dynamic nuclear polarization, J. Magn. Reson. 203 (2010) 138.
[36] M.-T. Türke, I. Tkach, M. Reese, P. Höfer, M. Bennati, Optimization of dynamic nuclear polarization experiments in aqueous solution at 15 MHz/9.7 GHz: a comparative study with DNP at 140 MHz/94 GHz, Phys. Chem. Chem. Phys. 12 (2010) 5893.
[37] V.P. Denysenkov, M.J. Prandolini, A. Krahn, M. Gafurov, B. Endeward, T.F. Prisner, High-field DNP spectrometer for liquids, Appl. Magn. Reson. 34 (2008) 289.
[38] B.D. Armstrong, D.T. Edwards, R.J. Wylde, S.A. Walker, S. Han, A 200 GHz dynamic nuclear polarization spectrometer, Phys. Chem. Chem. Phys. 12 (2010) 5920.
[39] N.M. Loening, M. Rosay, V. Weis, R.G. Griffin, Solution-state dynamic nuclear polarization at high magnetic field, J. Am. Chem. Soc. 124 (2002) 8808.
[40] Q.Z. Ni, E. Daviso, T.V. Can, E. Markhasin, S.K. Jawla, T.M. Swager, et al., High frequency dynamic nuclear polarization, Acc. Chem. Res. 46 (2013) 1933.
[41] A.J. Rossini, A. Zagdoun, M. Lelli, A. Lesage, C. Copéret, L. Emsley, Dynamic nuclear polarization surface enhanced NMR spectroscopy, Acc. Chem. Res. 46 (2013) 1942.
[42] R. Gitti, C. Wild, C. Tsiao, K. Zimmer, T.E. Glass, H.C. Dorn, Solid liquid intermolecular transfer of dynamic nuclear-polarization—enhanced flowing fluid H-1-NMR signals via immobilized spin labels, J. Am. Chem. Soc. 110 (1988) 2294.
[43] M.D. Lingwood, T.A. Siaw, N. Sailasuta, B.D. Ross, P. Bhattacharya, S. Han, Continuous flow Overhauser dynamic nuclear polarization of water in the fringe field of a clinical magnetic resonance imaging system for authentic image contrast, J. Magn. Reson. 205 (2010) 247.
[44] A. Krahn, P. Lottmann, T. Marquardsen, A. Tavernier, M.-T. Türke, M. Reese, et al., Shuttle DNP spectrometer with a two-center magnet, Phys. Chem. Chem. Phys. 12 (2010) 5830.
[45] Ü. Akbey, W.T. Franks, A. Linden, M.O. Rydmark, S. Lange, H. Oschkinat, Dynamic nuclear polarization enhanced NMR in the solid-state, in: L.T. Kuhn (Ed.), Hyperpolarization Methods in NMR Spectroscopy, Springer, Berlin, Heidelberg, 2013, pp. 181–228.
[46] D.J. Lurie, S. Aime, S. Baroni, N.A. Booth, L.M. Broche, C.H. Choi, et al., Fast field-cycling magnetic resonance imaging, C. R. Phys. 11 (2010) 136.
[47] K.I. Matsumoto, S. Subramanian, R. Murugesan, J.B. Mitchell, M.C. Krishna, Spatially resolved biologic information from in vivo EPRI, OMRI, and MRI, Antioxid. Redox Sign. 9 (2007) 1125.
[48] D.J. Lurie, D.M. Bussell, L.H. Bell, J.R. Mallard, Proton electron double magnetic-resonance imaging of free-radical solutions, J. Magn. Reson. 76 (1988) 366.
[49] K. Shet, G.L. Caia, E. Kesselring, A. Samouilov, S. Petryakov, D.J. Lurie, et al., A novel variable field system for field-cycled dynamic nuclear polarization spectroscopy, J. Magn. Reson. 205 (2010) 202.
[50] C.R. Bowers, D.P. Weitekamp, Para-hydrogen and synthesis allow dramatically enhanced nuclear alignment, J. Am. Chem. Soc. 109 (1987) 5541.
[51] T.C. Eisenschmid, R.U. Kirss, P.P. Deutsch, S.I. Hommeltoft, R. Eisenberg, J. Bargon, et al., Para hydrogen induced polarization in hydrogenation reactions, J. Am. Chem. Soc. 109 (1987) 8089.
[52] L. Buljubasich, M.B. Franzoni, K. Münnemann, Parahydrogen induced polarization by homogeneous catalysis: theory and applications, Top. Curr. Chem. 338 (2013) 33.
[53] J. Natterer, O. Schedletzky, J. Barkemeyer, J. Bargon, S.J. Glaser, Investigating catalytic processes with parahydrogen: evolution of zero-quantum coherence in AA′X spin systems, J. Magn. Reson. 133 (1998) 92.

[54] S.B. Duckett, D. Blazina, The study of inorganic systems by NMR spectroscopy in conjunction with parahydrogen-induced polarisation, Eur. J. Inorg. Chem. 2003 (2003) 2901.
[55] S.B. Duckett, C.J. Sleigh, Applications of the parahydrogen phenomenon: a chemical perspective, Prog. Nucl. Magn. Reson. Spectrosc. 34 (1999) 71.
[56] I.V. Koptyug, K.V. Kovtunov, S.R. Burt, M.S. Anwar, C. Hilty, S.I. Han, et al., para-hydrogen-induced polarization in heterogeneous hydrogenation reactions, J. Am. Chem. Soc. 129 (2007) 5580.
[57] K.V. Kovtunov, I.E. Beck, V.I. Bukhtiyarov, I.V. Koptyug, Observation of parahydrogen-induced polarization in heterogeneous hydrogenation on supported metal catalysts, Angew. Chem. Int. Ed. 47 (2008) 1492.
[58] K.V. Kovtunov, V.V. Zhivonitko, A. Corma, I.V. Koptyug, Parahydrogen-induced polarization in heterogeneous hydrogenations catalyzed by an immobilized Au(III) complex, J. Phys. Chem. Lett. 1 (2010) 1705.
[59] L.S. Bouchard, K.V. Kovtunov, S.R. Burt, M.S. Anwar, I.V. Koptyug, R.Z. Sagdeev, et al., Para-hydrogen-enhanced hyperpolarized gas-phase magnetic resonance imaging, Angew. Chem. Int. Ed. 46 (2007) 4064.
[60] M. Goldman, H. Johannesson, Conversion of a proton pair para order into C-13 polarization by rf irradiation, for use in MRI, C. R. Phys. 6 (2005) 575.
[61] M. Goldman, H. Johannesson, O. Axelsson, M. Karlsson, Hyperpolarization of C-13 through order transfer from parahydrogen: a new contrast agent for MFI, Magn. Reson. Imaging 23 (2005) 153.
[62] F. Reineri, A. Viale, G. Giovenzana, D. Santelia, W. Dastru, R. Gobetto, et al., New hyperpolarized contrast agents for C-13-MRI from para-hydrogenation of oligooxyethylenic alkynes, J. Am. Chem. Soc. 130 (2008) 15047.
[63] M. Haake, J. Natterer, J. Bargon, Efficient NMR pulse sequences to transfer the parahydrogen-induced polarization to hetero nuclei, J. Am. Chem. Soc. 118 (1996) 8688.
[64] H. Sengstschmid, R. Freeman, J. Barkemeyer, J. Bargon, A new excitation sequence to observe the PASADENA effect, J. Magn. Reson. Ser. A 120 (1996) 249.
[65] H. Johannesson, O. Axelsson, M. Karlsson, Transfer of para-hydrogen spin order into polarization by diabatic field cycling, C. R. Phys. 5 (2004) 315.
[66] K.L. Ivanov, A.V. Yurkovskaya, H.M. Vieth, Coherent transfer of hyperpolarization in coupled spin systems at variable magnetic field, J. Chem. Phys. 128 (2008) 154701.
[67] S.E. Korchak, K.L. Ivanov, A.V. Yurkovskaya, H.M. Vieth, Para-hydrogen induced polarization in multi-spin systems studied at variable magnetic field, Phys. Chem. Chem. Phys. 11 (2009) 11146.
[68] M. Carravetta, M.H. Levitt, Long-lived nuclear spin states in high-field solution NMR, J. Am. Chem. Soc. 126 (2004) 6228.
[69] M. Carravetta, M.H. Levitt, Theory of long-lived nuclear spin states in solution nuclear magnetic resonance. I. Singlet states in low magnetic field, J. Chem. Phys. 122 (2005) 214505.
[70] T. Jonischkeit, U. Bommerich, J. Stadler, K. Woelk, H.G. Niessen, J. Bargon, Generating long-lasting H-1 and C-13 hyperpolarization in small molecules with parahydrogen-induced polarization, J. Chem. Phys. 124 (2006) 201109.
[71] P. Hübler, J. Bargon, S.J. Glaser, Nuclear magnetic resonance quantum computing exploiting the pure spin state of para hydrogen, J. Chem. Phys. 113 (2000) 2056.
[72] M.S. Anwar, D. Blazina, H.A. Carteret, S.B. Duckett, T.K. Halstead, J.A. Jones, et al., Preparing high purity initial states for nuclear magnetic resonance quantum computing, Phys. Rev. Lett. 93 (2004) 040501.
[73] M.S. Anwar, L. Xiao, A.J. Short, J.A. Jones, D. Blazina, S.B. Duckett, et al., Practical implementations of twirl operations, Phys. Rev. A 71 (2005) 032327.

[74] R.W. Adams, J.A. Aguilar, K.D. Atkinson, M.J. Cowley, P.I. Elliott, S.B. Duckett, et al., Reversible interactions with para-hydrogen enhance NMR sensitivity by polarization transfer, Science 323 (2009) 1708.
[75] K.D. Atkinson, M.J. Cowley, S.B. Duckett, P.I. Elliott, G.G. Green, J. Lopez-Serrano, et al., Para-hydrogen induced polarization without incorporation of para-hydrogen into the analyte, Inorg. Chem. 48 (2009) 663.
[76] E.R. McCarney, S. Han, Spin-labeled gel for the production of radical-free dynamic nuclear polarization enhanced molecules for NMR spectroscopy and imaging, J. Magn. Reson. 190 (2008) 307.
[77] I. Solomon, Relaxation processes in a system of 2 spins, Phys. Rev. 99 (1955) 559.
[78] P.S. Hubbard, Theory of electron-nucleus Overhauser effects in liquids containing free radicals, Proc. R. Soc. Lond. Ser. A 291 (1966) 537.
[79] M. Bennati, C. Luchinat, G. Parigi, M.-T. Türke, Water H-1 relaxation dispersion analysis on a nitroxide radical provides information on the maximal signal enhancement in Overhauser dynamic nuclear polarization experiments, Phys. Chem. Chem. Phys. 12 (2010) 5902.
[80] M.-T. Türke, M. Bennati, Saturation factor of nitroxide radicals in liquid DNP by pulsed ELDOR experiments, Phys. Chem. Chem. Phys. 13 (2011) 3630.
[81] D. Sezer, M.J. Prandolini, T.F. Prisner, Dynamic nuclear polarization coupling factors calculated from molecular dynamics simulations of a nitroxide radical in water, Phys. Chem. Chem. Phys. 11 (2009) 6626.
[82] O. Neudert, C. Mattea, H.W. Spiess, S. Stapf, K. Münnemann, A comparative study of 1H and 19F Overhauser DNP in fluorinated benzenes, Phys. Chem. Chem. Phys. 15 (2013) 20717.
[83] B.C. Dollmann, M.J.N. Junk, M. Drechsler, H.W. Spiess, D. Hinderberger, K. Münnemann, Thermoresponsive, spin-labeled hydrogels as separable DNP polarizing agents, Phys. Chem. Chem. Phys. 12 (2010) 5879.
[84] Y. Cao, X.X. Zhu, J.T. Luo, H.Y. Liu, Effects of substitution groups on the RAFT polymerization of N-Alkylacrylamides in the preparation of thermosensitive block copolymers, Macromolecules 40 (2007) 6481.
[85] M.J.N. Junk, U. Jonas, D. Hinderberger, EPR spectroscopy reveals nanoinhomogeneities in the structure and reactivity of thermoresponsive hydrogels, Small 4 (2008) 1485.
[86] E.R. McCarney, B.D. Armstrong, M.D. Lingwood, S. Han, Hyperpolarized water as an authentic magnetic resonance imaging contrast agent, Proc. Natl. Acad. Sci. USA 104 (2007) 1754.
[87] K. Münnemann, C. Bauer, J. Schmiedeskamp, H.W. Spiess, W.G. Schreiber, D. Hinderberger, A mobile DNP polarizer for clinical applications, Appl. Magn. Reson. 34 (2008) 321.
[88] O. Neudert, D.G. Zverev, C. Bauer, P. Blümler, H.W. Spiess, D. Hinderberger, et al., Overhauser DNP and EPR in a mobile setup: influence of magnetic field inhomogeneity, Appl. Magn. Reson. 43 (2012) 149.
[89] C. Bauer, H. Raich, G. Jeschke, P. Blumler, Design of a permanent magnet with a mechanical sweep suitable for variable-temperature continuous-wave and pulsed EPR spectroscopy, J. Magn. Reson. 198 (2009) 222.
[90] H.C. Dorn, R. Gitti, K.H. Tsai, T.E. Glass, The flow transfer of a bolus with H-1 dynamic nuclear polarization from low to high magnetic fields, Chem. Phys. Lett. 155 (1989) 227.
[91] M. Utz, J. Landers, Magnetic resonance and microfluidics, Science 330 (2010) 1056.
[92] S. Stevenson, T. Glass, H.C. Dorn, C-13 dynamic nuclear polarization: an alternative detector for recycled-flow NMR experiments, Anal. Chem. 70 (1998) 2623.

[93] J. Natterer, J. Bargon, Parahydrogen induced polarization, Prog. Nucl. Magn. Reson. Spectrosc. 31 (1997) 293.
[94] M.G. Pravica, D.P. Weitekamp, Net Nmr alignment by adiabatic transport of para-hydrogen addition-products to high magnetic-field, Chem. Phys. Lett. 145 (1988) 255.
[95] M.H. Levitt, Spin Dynamics: Basics of Nuclear Magnetic Resonance, second ed., John Wiley & Sons, Chichester, 2008.
[96] D. Canet, C. Aroulanda, P. Mutzenhardt, S. Aime, R. Gobetto, F. Reineri, Para-hydrogen enrichment and hyperpolarization, Concepts Magn. Reson. A 28A (2006) 321.
[97] L. Buljubasich, I. Prina, M.B. Franzoni, K. Münnemann, H.W. Spiess, R.H. Acosta, High resolution para-hydrogen induced polarization in inhomogeneous magnetic fields, J. Magn. Reson. 230 (2013) 155.
[98] A. Allerhand, Analysis of Carr-Purcell spin-echo NMR experiments on multiple-spin systems. I. The effect of homonuclear coupling, J. Chem. Phys. 44 (1966) 1.
[99] R.R. Ernst, G. Bodenhausen, A. Wokaun, Principles of Nuclear Magnetic Resonance in One and Two Dimensions, Oxford University Press, New York, 1987.
[100] E. Fukushima, S.B.W. Roeder, N.M.R. Pulse, Experimental Pulse NMR: A nuts and Bolts Approach, Addison-Wesley, Reading, Massachusetts, 1981.
[101] R. Freeman, H.D.W. Hill, High-resolution study of NMR spin echoes: "J Spectra", J. Chem. Phys. 54 (1971) 301.
[102] J.A. Tang, F. Gruppi, R. Fleysher, D.K. Sodickson, J.W. Canary, A. Jerschow, Extended para-hydrogenation monitored by NMR spectroscopy, Chem. Commun. 47 (2011) 958–960.
[103] T. Gullion, D.B. Baker, M.S. Conradi, New, compensated Carr-Purcell sequences, J. Magn. Reson. 89 (1990) 479.
[104] S. Mansson, E. Johansson, P. Magnusson, C.M. Chai, G. Hansson, J.S. Petersson, et al., C-13 imaging - a new diagnostic platform, Eur. Radiol. 16 (2006) 57.
[105] E.Y. Chekmenev, J. Hovener, V.A. Norton, K. Harris, L.S. Batchelder, P. Bhattacharya, et al., PASADENA hyperpolarization of succinic acid for MRI and NMR spectroscopy, J. Am. Chem. Soc. 130 (2008) 4212.
[106] M. Roth, A. Koch, P. Kindervater, J. Bargon, H.W. Spiess, K. Münnemann, C-13 hyperpolarization of a barbituric acid derivative via parahydrogen induced polarization, J. Magn. Reson. 204 (2010) 50.
[107] R. Sarkar, P.R. Vasos, G. Bodenhausen, Singlet-state exchange NMR spectroscopy for the study of very slow dynamic processes, J. Am. Chem. Soc. 129 (2007) 328.
[108] E. Vinogradov, A.K. Grant, Long-lived states in solution NMR: selection rules for intramolecular dipolar relaxation in low magnetic fields, J. Magn. Reson. 188 (2007) 176.
[109] K. Gopalakrishnan, G. Bodenhausen, Lifetimes of the singlet-states under coherent off-resonance irradiation in NMR spectroscopy, J. Magn. Reson. 182 (2006) 254.
[110] L. Frydman, Chemistry awakens a silent giant, Nat. Chem. 1 (2009) 176.
[111] T. Theis, P. Ganssle, G. Kervern, S. Knappe, J. Kitching, M.P. Ledbetter, et al., Parahydrogen-enhanced zero-field nuclear magnetic resonance, Nat. Phys. 7 (2011) 571.
[112] P.R. Vasos, A. Comment, R. Sarkar, P. Ahuja, S. Jannin, J.P. Ansermet, et al., Long-lived states to sustain hyperpolarized magnetization, Proc. Natl. Acad. Sci. USA 106 (2009) 18469.
[113] Y.S. Feng, T. Theis, X.F. Liang, Q. Wang, P. Zhou, W.S. Warren, Storage of hydrogen spin polarization in long-lived C-13(2) singlet order and implications for hyperpolarized magnetic resonance imaging, J. Am. Chem. Soc. 135 (2013) 9632.

[114] G. Pileio, S. Bowen, C. Laustsen, M.C.D. Tayler, J.T. Hill-Cousins, L.J. Brown, et al., Recycling and imaging of nuclear singlet hyperpolarization, J. Am. Chem. Soc. 135 (2013) 5084.
[115] F. Hund, On the explanation of molecular spectra I, Z. Phys. 40 (1927) 742.
[116] L.D. Landau, Zur Theorie der Energieübertragung bei Stößen II, Phys. Z. Sowjet. 2 (1932) 46.
[117] C. Zener, Non-adiabatic crossing of energy levels, Proc. R. Soc. Lond. Ser. A 137 (1932) 696.
[118] J.A. Pople, W.G. Schneider, H.J. Bernstein, The analysis of nuclear magnetic resonance spectra: II. Two pairs of two equivalent nuclei, Can. J. Chem. 35 (1957) 1060.
[119] K. Miesel, K.L. Ivanov, A.V. Yurkovskaya, H.M. Vieth, Coherence transfer during field-cycling NMR experiments, Chem. Phys. Lett. 425 (2006) 71.
[120] M. Roth, P. Kindervater, H.P. Raich, J. Bargon, H.W. Spiess, K. Münnemann, Continuous H-1 and C-13 signal enhancement in NMR spectroscopy and MRI using parahydrogen and hollow-fiber membranes, Angew. Chem. Int. Ed. 49 (2010) 8358.
[121] K. Münnemann, M. Kölzer, I. Blakey, A.K. Whittaker, K.J. Thurecht, Hyperbranched polymers for molecular imaging: designing polymers for parahydrogen induced polarisation (PHIP), Chem. Commun. 48 (2012) 1583.